

University of Denver

Digital Commons @ DU

---

Electronic Theses and Dissertations

Graduate Studies

---

1-1-2016

## Design and Development of an Air Supply System for an Unmanned Circulation Control Aerial Vehicle

Pranith Chander Saka  
*University of Denver*

Follow this and additional works at: <https://digitalcommons.du.edu/etd>



Part of the [Engineering Commons](#)

---

### Recommended Citation

Saka, Pranith Chander, "Design and Development of an Air Supply System for an Unmanned Circulation Control Aerial Vehicle" (2016). *Electronic Theses and Dissertations*. 1268.  
<https://digitalcommons.du.edu/etd/1268>

This Thesis is brought to you for free and open access by the Graduate Studies at Digital Commons @ DU. It has been accepted for inclusion in Electronic Theses and Dissertations by an authorized administrator of Digital Commons @ DU. For more information, please contact [jennifer.cox@du.edu](mailto:jennifer.cox@du.edu), [dig-commons@du.edu](mailto:dig-commons@du.edu).

---

# Design and Development of an Air Supply System for an Unmanned Circulation Control Aerial Vehicle

## Abstract

Small-scale Unmanned Aerial Vehicles (UAVs) have been used for decades and are increasing in number and effectiveness as aircraft, sensor and automation technologies mature. Since the demand for UAV platforms capable of performing multiple missions with enhanced performance is increasing, technologies as Circulation Control (CC), which is an active flow control technique that is used to achieve enhanced payload and aerodynamic efficiency, attracts the interest of the research community. This thesis describes the design, development, integration and testing (ground and flight testing) of a CC system capable to provide the required mass flow for a CC-based flight. Performance evaluation is conducted at individual component level and at overall system level using computational fluid dynamics analysis and experimental testing. The CC system, when integrated on-board the UAV, can achieve momentum coefficient of blowing (C) ranging from 0.009 to 0.05 depending on the application. Flight testing results validate the performance of the system and indicate that CC can be applied effectively on small-scale UAVs, overcoming space and power limitations.

## Document Type

Thesis

## Degree Name

M.S.

## Department

Electrical Engineering

## First Advisor

Kimon P. Valavanis, Ph.D.

## Second Advisor

Matthew J. Rutherford, Ph.D.

## Third Advisor

Corinne Lengsfeld

## Keywords

Air supply system, Unmanned circulation control aerial vehicle

## Subject Categories

Engineering

## Publication Statement

Copyright is held by the author. User is responsible for all copyright compliance.

Design and Development of an Air Supply System for an Unmanned Circulation Control  
Aerial Vehicle

---

A Thesis

Presented to

the Faculty of the Daniel Felix Ritchie School of Engineering and Computer Science

University of Denver

---

In Partial Fulfillment

of the Requirements for the Degree

Master of Science

---

by

Pranith Chander Saka

August 2016

Advisors: Kimon P. Valavanis, Ph.D. and Matthew J. Rutherford, Ph.D.

Author: Pranith Chander Saka

Title : Design and Development of an Air Supply System for an Unmanned Circulation Control Aerial Vehicle

Advisors : Kimon P. Valavanis, Ph.D. and Matthew J. Rutherford, Ph.D.

Degree Date : August 2016

## **Abstract**

Small-scale Unmanned Aerial Vehicles (UAVs) have been used for decades and are increasing in number and effectiveness as aircraft, sensor and automation technologies mature. Since the demand for UAV platforms capable of performing multiple missions with enhanced performance is increasing, technologies as Circulation Control (CC), which is an active flow control technique that is used to achieve enhanced payload and aerodynamic efficiency, attracts the interest of the research community. This thesis describes the design, development, integration and testing (ground and flight testing) of a CC system capable to provide the required mass flow for a CC-based flight. Performance evaluation is conducted at individual component level and at overall system level using computational fluid dynamics analysis and experimental testing. The CC system, when integrated on-board the UAV, can achieve momentum coefficient of blowing ( $C_{\mu}$ ) ranging from 0.009 to 0.05 depending on the application. Flight testing results validate the performance of the system and indicate that CC can be applied effectively on small-scale UAVs overcoming space and power limitations.

# Acknowledgments

This thesis became a reality with the support and help of many individuals. I would like to extend my sincere thanks to all of them.

Foremost, I want to offer this endeavor to God Almighty for the wisdom, peace of mind, strength he bestowed upon me in order to complete this research.

To my parents Prasad and Sunitha and my brother Prathik, who have provided unequivocal support, strength and sacrifice throughout, for which my mere expression of thanks would not suffice.

My thanks to my advisors Dr. Kimon P. Valavanis and Dr. Rutherford, for the orientation through the contents of this thesis, and for imparting their knowledge and expertise in this study.

To all my colleagues and friends, for their encouragement, guidance and support through the years. A special thanks to all my colleagues at the University of Denver Unmanned Systems Research Institute. This research was partially supported by NSF Grants CNS-1229236 and CNS-1446285.

# Table of Contents

<b>1</b>	<b>Introduction</b>	<b>1</b>
1.1	Motivation . . . . .	2
1.2	Problem Statement . . . . .	2
1.3	Methodology . . . . .	3
1.4	Summary of Contributions . . . . .	4
1.5	Organization of the Thesis . . . . .	5
<b>2</b>	<b>Literature Review</b>	<b>6</b>
2.1	Circulation Control Applications . . . . .	7
2.2	Centrifugal Compressors . . . . .	13
2.3	Remarks . . . . .	16
<b>3</b>	<b>Air Supply Unit</b>	<b>18</b>
3.1	Introduction . . . . .	18
3.2	Centrifugal Compressors . . . . .	18
3.2.1	Dimensional Analysis of a Centrifugal Compressor . . . . .	21
3.2.2	One Dimensional Flow Analysis . . . . .	22
3.3	Design Methodology . . . . .	26
3.4	Model(s) Description . . . . .	33
3.4.1	Generation-I . . . . .	33
3.4.2	Generation-II . . . . .	35
3.5	Performance characterization . . . . .	37
3.5.1	Instrumentation . . . . .	38
3.5.2	Experimental Setup . . . . .	40
3.5.3	Experimental Testing . . . . .	43
<b>4</b>	<b>Circulation Control System Integration</b>	<b>47</b>
4.1	Intake Duct Design . . . . .	48
4.2	Junction Design and Analysis . . . . .	50
4.3	Plenum Design and Analysis . . . . .	53
4.4	CC System Integration . . . . .	55

<b>5</b>	<b>UC<sup>2</sup>AV Results</b>	<b>60</b>
5.1	UC <sup>2</sup> AV Design . . . . .	60
5.1.1	Circulation Control Wing . . . . .	62
5.1.2	Flight Controls and Instrumentation . . . . .	64
5.2	Preflight Tests . . . . .	66
5.2.1	Flow Uniformity . . . . .	67
5.2.2	$C_{\mu}$ characterization . . . . .	68
5.3	UC <sup>2</sup> AV : Flight Results . . . . .	69
5.3.1	Take-off Characteristics . . . . .	69
<b>6</b>	<b>Conclusions and Future Work</b>	<b>73</b>
6.1	Conclusions . . . . .	73
6.2	Future Work . . . . .	74
	<b>Bibliography</b>	<b>74</b>

# List of Tables

3.1	Advantages and disadvantages of different classes of impellers of a centrifugal compressor. . . . .	20
4.1	K factors for the four junctions at different inlet velocities. . . . .	53
5.1	Dimensional specifications of the RMRC Anaconda . . . . .	61
5.2	Geometric parameters of the wing[1]. . . . .	63
5.3	Instrumentation/Sensor Specifications for UC <sup>2</sup> AV[1]. . . . .	65
5.4	CC flight test data. . . . .	70

# List of Figures

1.1 Prediction of the take-off performance of the UC2AV due to enhanced lift using CC. . . . .	3
2.1 Component layout and details of the Deamon UAV [2]. . . . .	7
2.2 Pneumatic component layout on the Deamon UAV. [3]. . . . .	8
2.3 Component layout and details of the PTERA C3 configuration [4]. . . . .	9
2.4 Details of the pneumatic system with in the CEETA PTERA-C3 configuration [4].	10
2.5 Component layout and details of the Amelia wind tunnel model [5]. . . . .	11
2.6 Pneumatic distribution system on side of the AMELIA model. [5]. . . . .	12
2.7 Internal pneumatic plumbing of the FAST-MAC[6]. . . . .	13
3.1 Components of a Centrifugal Compressor. . . . .	19
3.2 Head vs. flow relation of a centrifugal compressor [7]. . . . .	20
3.3 Generalized compressor map for compressor selection [7]. . . . .	22
3.4 Design and experimental validation flowchart. . . . .	28
3.5 Numerical estimation of blade angle ( $\beta_1$ ) and Mach Number at the impeller inlet ( $M_{r1}$ ) at inlet using mass flow function at zero prewhirl angle. . . . .	31
3.6 Different impeller configurations of generation-I ASU. . . . .	34
3.7 Different housing designs generation-I ASU. . . . .	35
3.8 Assembly of the generation-I ASU. . . . .	35
3.9 CAD design of the generation-II ASU. . . . .	36
3.10 Various components of the generation-II ASU. . . . .	36
3.11 Performance curve of the ASU at 10,000 RPM. . . . .	37
3.12 Calibrated pitot probe with an inner diameter of 0.3 mm. . . . .	38
3.13 Left: The airspeed sensor (pitot tube). Center: The Hitec servo programmer and controller. Right: The Hall effect sensor. <sup>2</sup> . . . . .	39
3.14 Schematic of the location of the sensors. . . . .	40
3.15 The experimental setup of the ASU. . . . .	42
3.16 The controller unit for the ASU. . . . .	43
3.17 Compressor map of the ASU. . . . .	44
3.18 Velocity distribution at the ASU outlet. . . . .	45
3.19 Experimental and simulation data of the ASU performance at different RPM. . . .	46
4.1 Schematic representation of the Circulation Control System. . . . .	48

---

<sup>2</sup><http://www.eagletreesystems.com>

4.2	CAD design integration of the fuselage, the ASU and the intake duct. . . . .	49
4.3	Contours of the flow field in the intake duct at 10 m/s inlet velocity. . . . .	49
4.4	CAD designs of junction configurations [8]. . . . .	51
4.5	Velocity contour of the junctions at 50 m/s inlet velocity from CFD analysis[8]. . .	51
4.6	CFD analysis on the four junction designs. The recorded pressure drop for different velocities is presented [8]. . . . .	52
4.7	Plenum CAD design: The vanes at the inlet are for flow correction and the vanes in the diffuser achieve uniformity. Nine standoffs are placed to avoid slot deformation during plenum pressurization[9]. . . . .	54
4.8	Flow uniformity performance across the span of the wing[9]. . . . .	55
4.9	CAD model of the CC system [8]. . . . .	56
4.10	The experimental setup of the CC system. . . . .	57
4.11	Experimental results representing the performance of the $V_{jet}$ at the slot across the span on each plenum for different RPM values. The deviation of the $V_{jet}$ from the average line (shown in black) at each RPM value is shown. . . . .	58
4.12	CFD analysis of the plenum designs. . . . .	58
4.13	CFD analysis off the plenum designs. . . . .	59
5.1	The RMRC Anaconda UAV platform. . . . .	61
5.2	The subsystems on-board the UC <sup>2</sup> AV. . . . .	62
5.3	The internal structure of the Circulation Control Wing.[1] . . . . .	63
5.4	Overview of the instrumentation system of the UC <sup>2</sup> AV[1]. . . . .	65
5.5	The UC <sup>2</sup> AV placed on the a stationary mount for platform. . . . .	66
5.6	Average jet velocity at different points across the span of the UC <sup>2</sup> AV. . . . .	67
5.7	The average $C_{\mu}$ at different RPM. . . . .	68
5.8	The UC <sup>2</sup> Av place on the runway prior to take-off.. . . .	69
5.9	Representation of the ground and air phase of take-off. . . . .	70
5.10	Take-off flight data. . . . .	71

# Nomenclature

$\omega$	Angular Velocity ( $rad/s$ )
$a$	Area of the impeller( $mm^2$ )
$A$	Area ( $mm^2$ )
$t$	Blade Thickness ( $mm$ )
$c$	Chord ( $mm$ )
$A$	Cross-section area ( $mm^2$ )
$I$	Current ( <i>Ampere</i> )
$\rho$	Density of air ( $kg/m^3$ )
$D$	Diameter ( $mm$ )
$q_\infty$	Dynamic pressure
$C_D$	Finite wing drag coefficient
$C_L$	Finite wing lift coefficient
$\phi$	Flow Coefficient
$Q$	Flow-rate ( $m^3/s$ )
$f$	Friction factor
$R$	Gas constant ( $J/K - mol$ )
$H$	Head ( $mm$ )
$\psi$	Head Coefficient
$\beta$	Impeller Blade Angle (Degrees)

$\Delta$	Incremental change
$\alpha$	Inlet Flow Angle (Degrees)
$\mu$	Kinematic viscosity ( $m^2/s$ )
$L$	Length of the tubing ( $mm$ )
$\Delta C_L/C_\mu$	Lift augmentation ratio
$M$	Mach number
$\dot{m}$	Mass flow rate ( $kg/s$ )
$MTOW$	Maximum Take-off Weight (lbs)
$C_\mu$	Momentum Coefficient of Blowing
$P$	Pressure ( $KPa$ )
$U$	Radial Velocity ( $m/s$ )
$r$	Radius ( $mm$ )
$c_{ref}$	Reference chord ( $mm$ )
$Re$	Reynolds Number
$RPM$	Rotation Per Minute
$h$	Slot height ( $mm$ )
$D_s$	Specific Diameter
$g_c$	Specific gravity ( $kg/mm^3$ )
$C_p$	Specific Heat ( $J/kg - K$ )
$N_s$	Specific Speed
$\gamma$	Specific Weight of the Fluid ( $N/m^3$ )
$N$	Speed ( $RPM$ )
$V_\theta$	Tangential Velocity ( $m/s$ )
$T$	Temperature ( <i>Celsius</i> )
$UC^2AV$	Unmanned Circulation Control Aerial Vehicle

$V$	Velocity ( $m^2/s$ )
$V$	Voltage ( <i>Volt</i> )
$b$	Wing span ( $mm$ )
$S$	Wing surface area ( $mm^2$ )

### **Subscript**

<i>in</i>	Inlet
<i>jet</i>	Jet
<i>m</i>	mean
<i>out</i>	Outlet
<i>s</i>	Static

# Chapter 1

## Introduction

The research in the field of aviation has expanded the versatility and variety of small Unmanned Aerial Vehicles (UAVs). However, the limitation of payload capacity, infrastructure to take-off and land and limited flight duration, have restricted their applications from spreading into wider frontiers. Hence, in recent years the need for revolutionary concepts to further enhance the aerodynamic characteristics of UAVs is of increasing interest. The use of pneumatic control aerodynamic high lift configurations has been under research for over 60 years, and has shown potential to drastically improve aircraft systems [10, 11, 12, 13]. Circulation Control (CC) is an active flow control technique and has found its best application as a method of lift augmentation. The application of CC on Class-I UAVs (Maximum take-off weight  $< 20$  lbs) to enhance their performance is challenging due to the high energy and high mass flow of air that is required. In order to implement CC additional pneumatic components are required on board. The restriction in space, power and payload on-board adds constraints to the pneumatic source and delivery system. This thesis summarizes research to design, develop and test a pneumatic system to support CC on the Unmanned Circulation Control Aerial Vehicle (UC<sup>2</sup>AV).

## 1.1 Motivation

The idea of Coanda driven CC, which is an active flow control approach is proven to be the most effective method for lift enhancement when compared to traditional lift augmentation devices[14, 12, 13]. Kanistras et. al. [9] indicates that a NACA0015 Circulation Control Wing (CCW) can achieve a lift augmentation of up to 0.89 ( $C_l$ ) using a dual radius flap and upper slot TE blowing in a wind tunnel environment. Literature reveals the complexity in the design of a pneumatic source to apply CC on a Class-I UAV, and thus only a few UAVs have taken flight using CC applications. The following research questions have motivated this work:

- Is it feasible to use a centrifugal compressor-based pneumatic power source to meet the mass flow requirements of CC?
- Can rapid prototyping be used as an alternative method to manufacture a light weight pneumatic system?
- What are the steps, constraints and considerations during the design of a pneumatic system to support CC ?

## 1.2 Problem Statement

The implementation of CC on-board small-scale unmanned aircraft has challenges due to payload, space and power constraints. The problem statement for this research focuses around (i) the need for a pneumatic power source which can deliver high mass flow of high energy air; (ii) the need for a system to deliver the air from the pneumatic source to the CC slot uniformly with minimized losses and influence on the ASU performance; and (iii) The need for accurate instrumentation to test the performance of the various components.

The end goal of the research is the development of the UC<sup>2</sup>AV to efficiently augment lift using CC and thereby achieving reduced run way distances and increased payload capabilities. The predicted take-off characteristic of the UC<sup>2</sup>AV is shown in Figure 1.1.

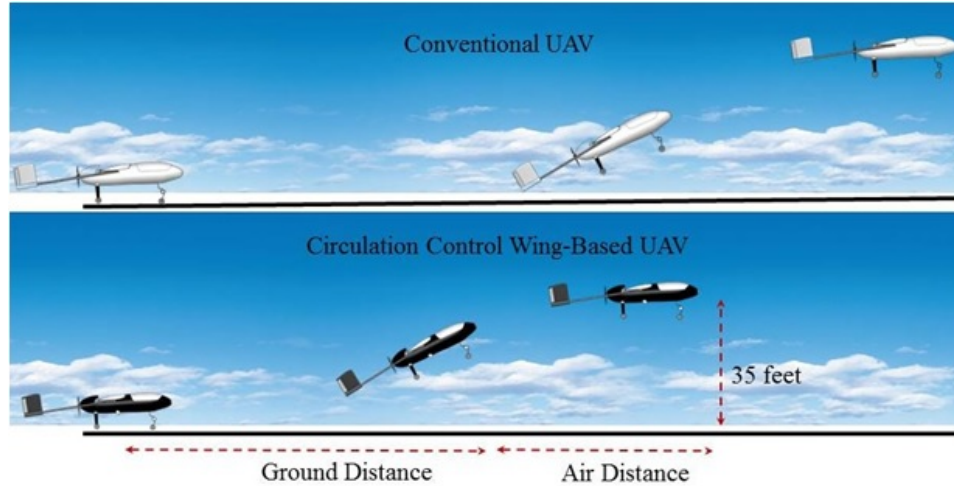


Figure 1.1: Prediction of the take-off performance of the UC<sup>2</sup>AV due to enhanced lift using CC.

### 1.3 Methodology

To tackle the challenges of achieving CC on-board a Class-I UAV, the research methodology focuses on the design and development of a light weight and compact pneumatic power source capable of providing the high energy and high mass flow of air. Centrifugal compressor configurations are tested to function as the pneumatic power source, called the Air Supply Unit (ASU). For the design and testing of the ASU a method of approach which includes 1-D optimization; CFD analysis to validate the theoretical design; 3-D rapid prototyping and testing of various compressor configurations is proposed. Research also focuses on the design, simulation and testing of a pneumatic delivery system called the Air Delivery System (ADS), which affects the compressor's performance. The ADS consists of: (i) the inlet ducting passage; (ii) the internal ducting that connects the ASU to the plenum; and (iii) the plenum, which is responsible for delivering the mass flow across the span. The

research to achieve uniform flow for CCWs is based of work by Kanistras et. al. in [9, 15], where a design that can distribute air uniformly across the span is presented. This work is taken as a baseline model and further design changes are made to the plenum design to minimize losses for efficient functioning of the ASU.

## 1.4 Summary of Contributions

The primary contribution of this work is the development and evaluation of a CC system for the Unmanned Circulation Control Aerial Vehicle ( $UC^2AV$ ). This  $UC^2AV$  is the first of its kind CC based airplane to demonstrate enhanced performance during flight testing. The main achievements and contributions are summarized as follows:

- Determine the best fit configuration of a centrifugal compressor as a pneumatic power source to achieve CC on a Class-I UAV.
- Design and build a light weight ASU that can meet the mass flow requirements to achieve effective CC.
- Investigate a suitable design of pneumatic plumbing that can minimize losses.
- Design, build and test a CC system which is integrable on-board the  $UC^2AV$ .
- The CC system is capable of achieving a momentum coefficient of blowing ( $C_\mu$ ) of 0.05 on-board the UAV.

The other achievements and contributions can be summarized as follows:

- Design and build a CCW, consisting of internal tubing and plena, which ingrates with the dual radius flaps to the CC system.
- Build the  $UC^2AV$  and integrate the CC system and instrumentation system on-board.

- Reduction of runway take-off distance by 53% during flight testing.
- Design and build a diffuser-nozzle based plenum to form the slot and deliver the air uniformly across the dual radius flap.

## 1.5 Organization of the Thesis

The remainder of the thesis is organized as follows: Chapter 2 consists of the literature review, where background information on different approaches to apply CC for various applications, along with a summary of research on design, computational and experimental testing of centrifugal compressors. Chapter 3 presents theoretical background, a design methodology and primary experimental results of the ASU. Chapter 4 presents the details of design development and experimental/ computation testing of the CC system and its subcomponents. Chapter 4 also presents the overview of the CC system and integration on the system on-board the UAV. Chapter 5 presents the design of the UC<sup>2</sup>AV and results from flight testing of the UC<sup>2</sup>AV. Chapter 6 consists of the conclusions and recommendations for future work.

# Chapter 2

## Literature Review

Circulation Control (CC) is one of many active flow control techniques, which has been under investigation since the 1930's [14, 12, 13, 16]. Extensive research has been conducted to study the effects of CC on aerodynamic bodies; numerical and computational studies have been conducted to understand the effects of CC on flow fields, while wind tunnel tests have proven the efficiency of CC as a lift augmentation method [17, 18, 14, 12, 13, 16]. Although CC has been widely investigated and has found its way into a large number of applications, implementation of CC on Class-I UAVs (MTOW < 20 lbs) has not received much attention due to the space limitations within the UAV's fuselage, the power restrictions on-board the UAV and the complexity of the Circulation Control Wing's (CCW) geometry. The beginning of this section provides overview of research related to applications of CC on UAVs and scaled wind tunnel models and their pneumatic CC systems. The latter half of the section focuses on review of literature related to centrifugal compressors (their design methodology, performance and applications) as a potential Air Supply Unit (ASU).

## 2.1 Circulation Control Applications

The first attempt to apply CC on a diamond shape wing UAV was the Flapless Air-Vehicle Integrated Industrial Research (FLAVIIR) project, which was a five year research program among ten British universities. The main objective of this program was the development of technologies that can enable low-cost UAVs to be maintenance free, by replacing conventional control surfaces while retaining the performance characteristics of the aircraft [2, 3, 10]. **DEAMON** has CC based units which replace TE control surfaces for roll control, and a Coanda based Fluidic Thrust Vectoring (FTV) nozzle for pitch control. The FTV nozzle uses air-bleed from the turbojet main engine, while the Auxiliary Power Unit (APU) supplies the pressurized air to the CC devices. Figure 2.1 shows the complete component layout of the DEAMON UAV.

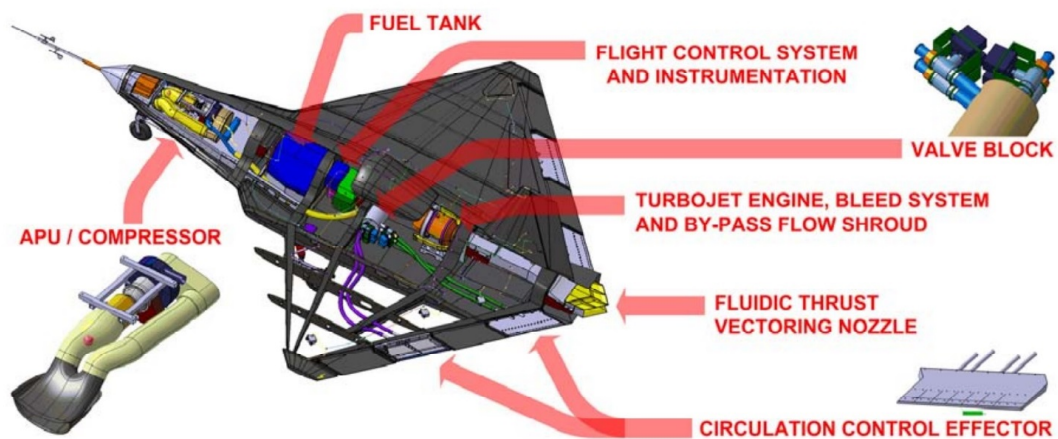


Figure 2.1: Component layout and details of the Deamon UAV [2].

The UAV has 4 CC units, where each unit requires 20 g/s mass flow of air, pressurized at 0.3- 0.5 bar for efficiency. The dedicated APU, which is the core of the pneumatic power generation system, consists of a micro turbojet engine driving a free power turbine, driving a compressor capable of delivering air at 90 g/s at 1.8 bar [3]. The APU draws air from the

inlet which is located at the bottom of the aircraft and transfers it to the distribution unit. Figure 2.2 shows the position of the APU and the pneumatic power distribution unit on-board the UAV. The pneumatic power distribution unit delivers the hot pressurized air from the APU at the front of the aircraft to the CC units. Flexible hi-purity teflon and nylon tubes along with valves weighing a total of 3.48 kg, are used for the air delivery, distribution and control system. Although the APU provides the required mass flow to the CC system, the drawbacks of such a system are the high temperature air which is provided by the turbine and the weight of the system.

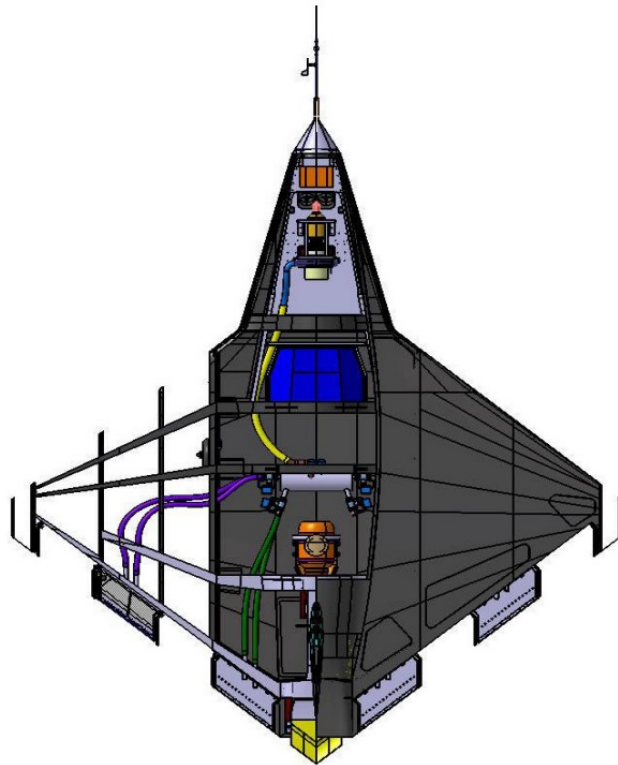


Figure 2.2: Pneumatic component layout on the Deamon UAV. [3].

**Cruise-Efficient Extreme Short Take-off and Landing (ESTOL) Transport Aircraft (CEETA)** demonstrator UAV Figure 2.3, which is a 10% scale B-737 aircraft, the Prototype-Technology Evaluator and Research Aircraft (PTERA-C3) configuration of this platform uses CC techniques for short take-off and landing (STOL) applications [4]. The

objective of the PTERA-C3 is to provide data, simulations and technology of a reconfigurable flight test vehicle for testing within the CC community.

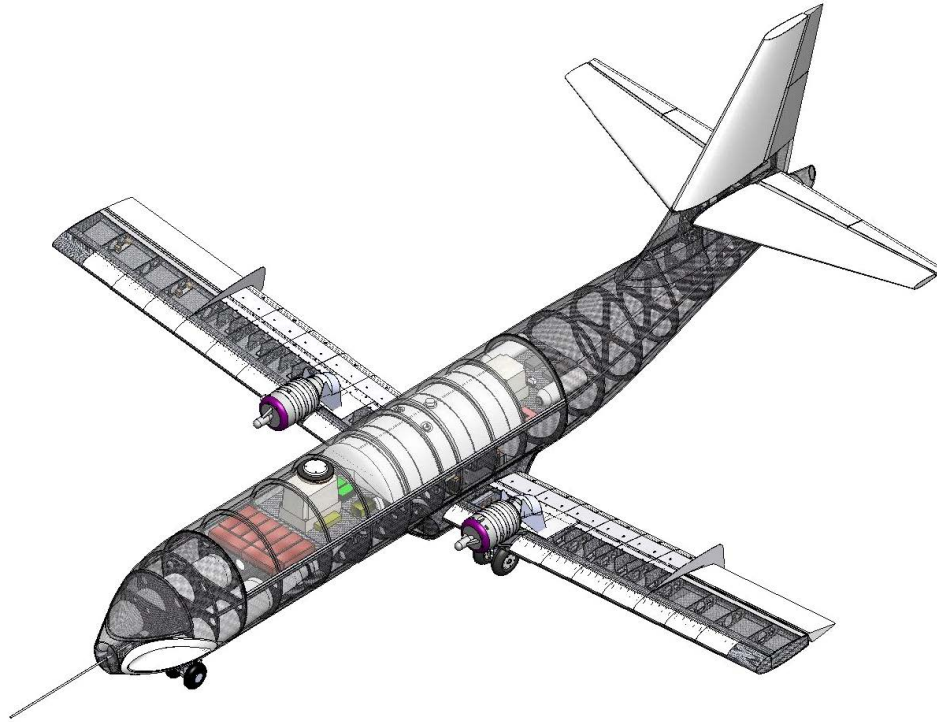


Figure 2.3: Component layout and details of the PTERA C3 configuration [4].

The Leading-Edge(LE) and Trailing-Edge(TE) blowing are used to achieve CC, along with over-the-wing power lift techniques to enhance the capabilities of the aircraft. Both the LE and TE plena and slots are supplied with the required mass flow by the auxiliary power unit (APU). The APU utilizes off-the-shelf Electric Ducted Fan (EDF) units (the Schubeler DS-94 HDT EDF), which function as axial compressors, to provide the pressure and mass flow for CC implementation and its interaction with over-the-wing powered lift assembly. Figure 2.4 depicts the pneumatic system and the location of the APU, also illustrating the flow distribution within the system. The two APUs have their respective inlet manifolds. The inlet manifold of the APU is strategically located on the ventral side of the fuselage close to the nose. Air moves in through the inlet manifolds and is then compressed by the

APU. Then the air from both APUs passes to the main duct before it is split to the LE and TE duct exits. The APU provides a  $C_{\mu} = 0.0153$  to the LE and  $C_{\mu} = 0.0660$  to the TE, at a total pressure ratio of 1.066 through a single plenum for a semi-span wing. The use of an EDF as a pneumatic source has drawbacks because of the low contraction ratio of the inlet and outlet plena as well as the large area inlet of the fans which modifies the flow field around the fuselage.

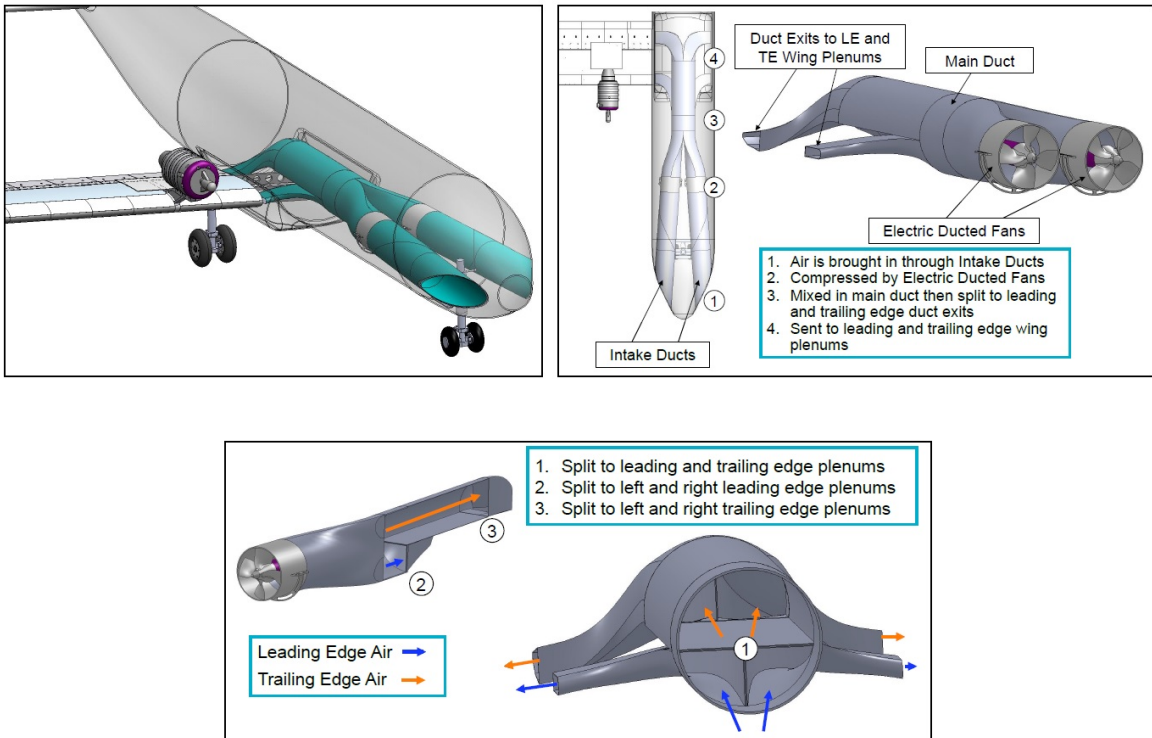


Figure 2.4: Details of the pneumatic system with in the CEETA PTERA-C3 configuration [4].

**The Advanced Model for Extreme Lift and Improved Aeroacoustics (AMELIA)** is a project by NASA Ames in collaboration with California Polytechnic State University and combines a Circulation Control Wing (CCW) with LE and TE blowing and over-the-wing engines to provide upper surface blowing and noise shielding [5]. The Computer Aided Design(CAD) model of the complete internal component layout is presented in Figure 2.5

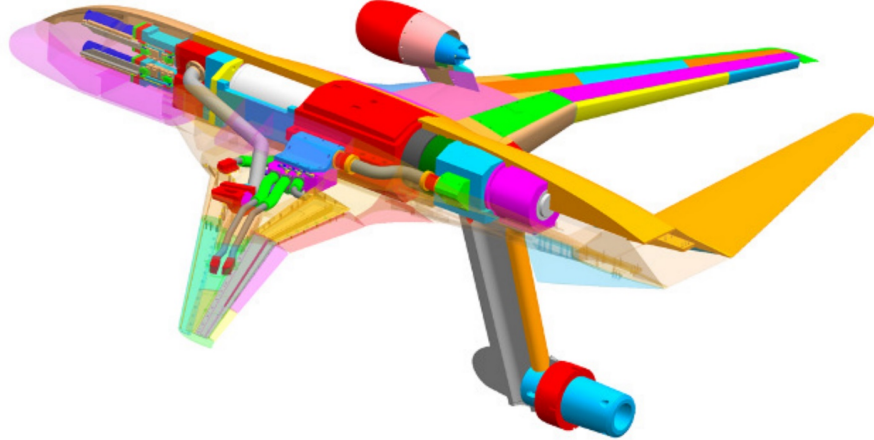


Figure 2.5: Component layout and details of the Amelia wind tunnel model [5].

AMELIA is a 1/11 scale wind tunnel model of a Cruise Efficient Short Take-off and Landing (CESTOL) aircraft. Since the wind tunnel model falls within the size scale of a Class-I UAV, the methodology of implementing CC can be easily adapted to a CC based Class-I UAV. AMELIA's air delivery system is a single plenum design. Minimizing breaks in the slot caused by plenum intersections was a high priority, to provide undisturbed flow across the upper surface and flaps. Each of the plenum designs is instrumented with three pressure probes and the aircraft is supplied using two separate air systems with internal piping for both the high (upper surface blowing) and low (leading and trailing-edge blowing) pressure systems [11]. The low pressure system (up to 100 psi) is used to supply air to the plena. The air is fed through a pipe attached to the underside of the sting, which disperses air to both wings through bellows, which is then delivered to the low pressure plena. Four butterfly valves are used to regulate the flow to the TE and LE slots. Several techniques to achieve flow uniformity along the span of the aircraft are tested and oil flow visualization is used to quantify the performance. Of the several techniques used to achieve flow uniformity, the 12% density metal foam with Rigimesh performed the best [19]. The

low pressure air distribution system for testing CC is shown in Figure 2.6. The challenges of using such a CC system, which is developed as a wind tunnel model for flow uniformity along the span is the required pressure ratio to support such a system. In this model an external stationary compressor provides the air to the system.

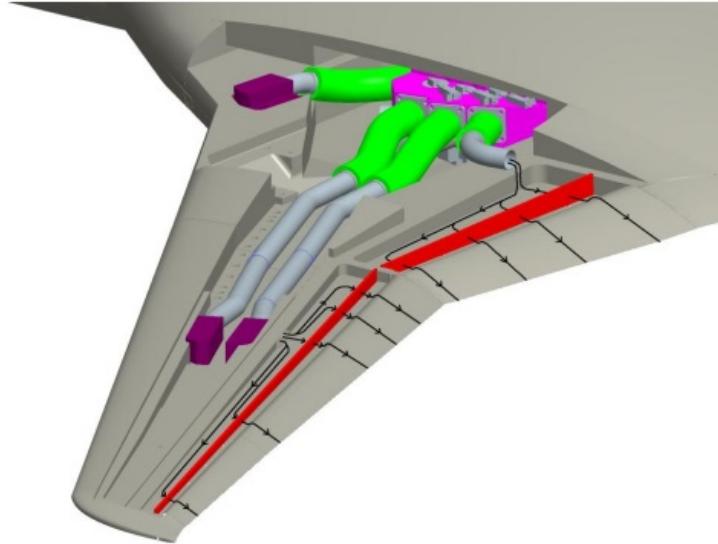


Figure 2.6: Pneumatic distribution system on side of the AMELIA model. [5].

NASA Langley Research Center is continuing research with the **Fundamental Aerodynamics Subsonic / Transonic Modular Active Control (FAST-MAC)** model in the National Transonic Facility focusing on viscous flow separation at full-scale Reynolds numbers [6]. Unlike AMELIA, which is a configuration, this is a generic research model, where in addition to high lift augmentation, focus is given on aerodynamic efficiency during cruise flight. FAST-MAC's air delivery system is more complicated than AMELIA's, since each flow path is divided into four sections along the span of the model. Each section has its own flow control valve located in the fuselage. Each plenum has four perforated plates designed to maintain flow uniformity since the flow is divided in four internal flow paths. The design of the perforated plates is critical because it establishes the maximum internal pressure, the maximum flow rate and it is responsible for the flow distribution along the

span [20]. Figure 2.7 shows the pneumatic distribution system of the FAST-MAC wind tunnel model.

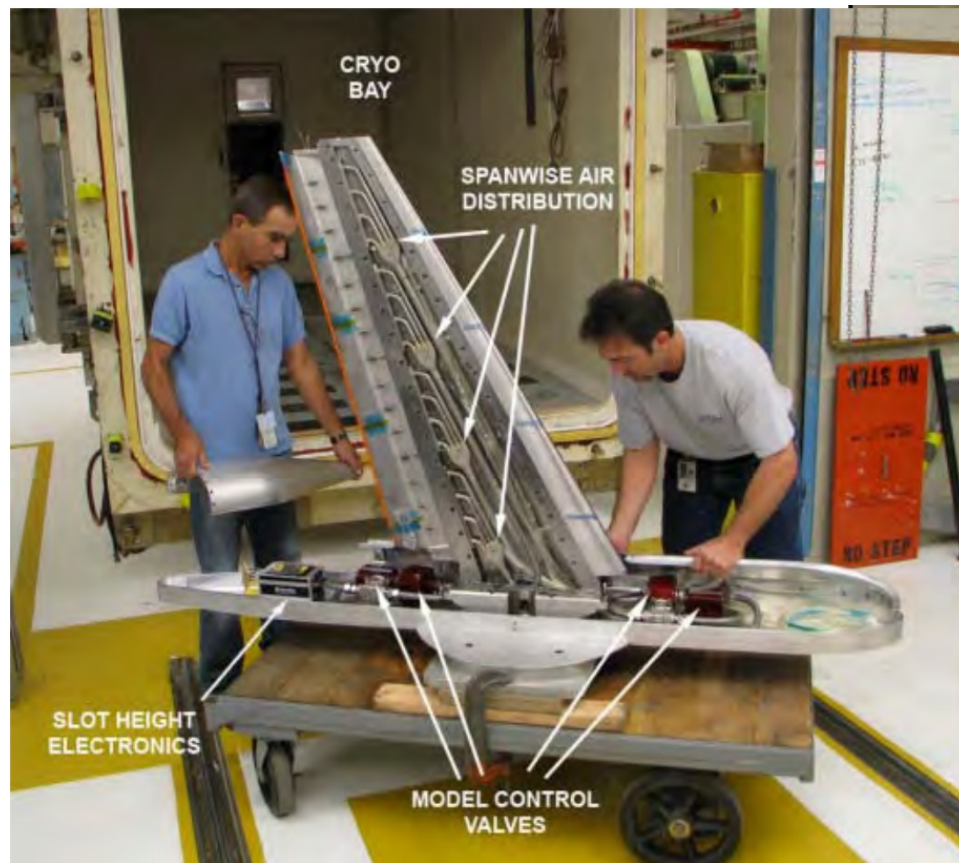


Figure 2.7: Internal pneumatic plumbing of the FAST-MAC[6].

## 2.2 Centrifugal Compressors

An air compressor is a mechanical device capable of transferring energy to air, so it can be delivered in large quantities at higher pressures [7]. Different types of fans and compressors have been used in the past to attain required mass flow on-board UAVs for CC based applications [3, 10, 4]. The primary difference between a fan and a compressor is the pressure ratio that can be achieved. Variable displacement compressors are of two kinds: axial and centrifugal compressors. Axial compressors are suitable for large flow applications at

low pressure, while centrifugal compressors are more commonly used for medium flow and higher pressure applications. Literature indicates [7, 21, 22] that centrifugal compressors can be used for a wide range of applications when high mass flow and pressure ratios are required.

Performance characteristics of an air supply system to pneumatically power the CCWs can be defined by two parameters: the mass flow rate and/or the moment coefficient of blowing ( $C_{\mu}$ ); and the pressure-ratio at which the air can be supplied to the TE of the CCW [23]. Palmer and Waterman [24] show that when a two-stage centrifugal compressor is used, high mass flow (3.3 kg/s) with a pressure ratio (14:1) can be achieved (T800-LHT-800 helicopter engine). However, Rahman and Scaringe [25] present experimental results of a small scale centrifugal compressor that is used for a refrigeration system, where the compressor operates at 18000 RPM with a pressure ratio of 1.045:1.

In [7], different types of compressor characteristics are analyzed and compared. The mathematical foundations and the principles of operation are explained in detail emphasizing that the impeller is the most crucial part of the compressor. The performance characteristics expected from the compressor are a function of the geometric parameters of the impeller, such as blade angle, vane profile, impeller radius and mode of impelling.

In [26], 1-D flow calculations are used to derive the principal dimensions of the centrifugal compressor's impeller, based on the required performance to reduce the design time. Then, a direct design procedure is used to arrive at a final design, which is later used in analysis of the compressor parameters. In [27], a similar design approach is adopted and additionally a MATLAB<sup>®</sup> <sup>1</sup> code is also implemented to determine geometric parameters of the impeller. The mass flow function used to optimize the design based on the expected performance of the compressor is given by:

---

<sup>1</sup><http://www.mathworks.com/>

$$\begin{aligned}
f(M_{rin}, \beta_{in}, \alpha_{in}) &= \frac{\dot{m}\omega^2}{\pi K P_{in} (\gamma R T_{in})^{1/2}} \\
&= \frac{M_{rin}^3 \cos^3 \beta_{in} (\tan \beta_{in} + \tan \alpha_{in})^2}{\left(1 + \frac{\gamma-1}{2} M_{rin}^2 \frac{\cos^2 \beta_{in}}{\cos^2 \alpha_{in}}\right)^{\frac{1}{\gamma-1} + \frac{3}{2}}}
\end{aligned} \tag{2.1}$$

where:

$$K = 1 - \left(\frac{r_{hin}}{r_{in}}\right)^2 \tag{2.2}$$

for zero degree prewhirl angle of the inlet velocity.

This 1-D formulation and analysis is an effective way to design a centrifugal compressor but, on the other hand, it does not account for parameters such as curve shape, slip, tolerances and the effect of splitter blades. In [28], an expanded optimization process of the mass flow equation (4.1) to other performance aspects of the centrifugal compressor is presented. A numerical code capable of calculating the range of input power, input torque, rotational speeds, mass flow rate, total pressure and temperature ratios for different sizes of impellers is developed and validated with experimental results.

In [29], a CFD analysis is carried out using ANSYS CFX to simulate the flow in an existing centrifugal compressor. The results are validated with respect to the performance parameters such as flow rate and pressure ratios. It is shown that with a commercially built compressor, the experimental results matched the CFD analysis with a deviation of 3%. This approach is being used by designers to make changes before manufacturing. In [30], a different approach is adopted to investigate the connection between the type of impeller to the compressor performance. Seven different designs of impellers and two designs of housings based on the impeller's are designed, developed and tested on the

basis of volumetric flow rate through the outlet of the compressor. Also, a Finite Element Analysis (FEA) is followed to check if the compressor operates in a safe region. It is further concluded that the best performance is achieved for the closed backward vane impeller.

In [31], a method for estimating the performance of a centrifugal compressor for a given application along with the aerodynamic modeling of actual compressor hardware is presented. It summarizes that Mach number effects and internal heat transfer are additional parameters, besides the actual impeller design, which can affect the accuracy of the aerodynamic model. In [32], a study on how the centrifugal compressor performance can be enhanced by introducing splitter vanes at selected locations is conducted. An extensive numerical analysis on the effect of splitter blades and the location of the blades is presented. In [33], research focuses on the application of 3-D inverse design method, aiming for a more efficient centrifugal compressor improving impeller's efficiency and pressure ratio without adverse effect on operating range. A structural analysis is conducted on a modified compressor in ANSYS, to compare the stress and vibration results of an existing turbocharger's impeller in order to optimize the design. The results confirm that the inverse designed impeller displayed improved stage efficiency and a pressure ratio improvement of 4.5% while maintaining or improving the compressor's operating range.

## **2.3 Remarks**

Literature reveals that although CC can achieve improved performance hence it can be applied to various applications (STOL characteristics, for roll and pitch control and noise reduction). Although due to the complexities in design and requirements of high energy and mass flow of air, only a few UAVs have successfully taken flight using CC. Various approaches have been adopted in the past to implement CC on UAVs or wind tunnel models. The models which have already been investigated cannot be directly implemented onto the

UC<sup>2</sup>AV mostly because of the weight restrictions, high temperature of air produced by the various designs of APUs and the geometric constraints which vary for each UAV model. Wind tunnel models on the other hand provide solutions to the method of distributing air and flow uniformity, but the models are heavy and require a large working pressure ratio to achieve efficiency. Although a few design methods similar to wind tunnel CCW models are considered for the UC<sup>2</sup>AV, due to the restriction on-board a novel approach of design and manufacture is adopted.

If CC is applied for high lift augmentation purposes, high velocities at the slot are required and centrifugal compressors can be designed and optimized to reach the performance that is required. Additionally, conventional centrifugal compressors are heavy due to the methods of their manufacture. However, using 3-D printing technology, the proposed light-weight centrifugal compressor can function as a ASU on-board a UAV for CC based applications. In conclusion, with an adequate design method and manufacturing technique, centrifugal compressors can be used to supply the required mass flow for efficient functioning of CCWs.

# Chapter 3

## Air Supply Unit

### 3.1 Introduction

The purpose of this chapter is to provide a detailed understanding of the Air Supply Unit (ASU). The ASU is essentially a centrifugal compressor, which is powered through a brushless motor and supplies the required mass flow of air to the CCW. The chapter focuses on (i) the aerodynamics of a centrifugal compressor; (ii) the method of approach for the design methodology and experimental testing of the compressor; (iii) the model tested for its performance with the proposed air delivery system for the efficient functioning of CCWs defined by Kanistras et. al. in [34].

### 3.2 Centrifugal Compressors

Centrifugal compressors, also known as radial compressors, derive their name from the direction of the fluid as it moves through the compressor. Centrifugal compressors are known to generate high pressure ratios and handle moderate mass flow of the working fluid, and have a wide variety of applications as stated in Chapter 2.

A centrifugal compressor includes the following components: inlet guide vanes, an inducer, the impeller, a diffuser, and a volute scroll for a single stage of compression as shown in Figure 3.1. The fluid enters the compressor from the inlet duct and is moved through the inlet guide vanes which provide the fluid with a pre-whirl angle. The inducer section of the compressor along with the impeller move the fluid from an axial direction at the inlet to a radial direction into the diffuser or volute scroll. The rotation of the impeller transfers kinetic energy to the fluid. As the fluid moves to the diffuser, the kinetic energy is converted to static pressure of the fluid. Then the fluid moves to the volute scroll, where the static pressure rises further before the fluid moves towards the exit.

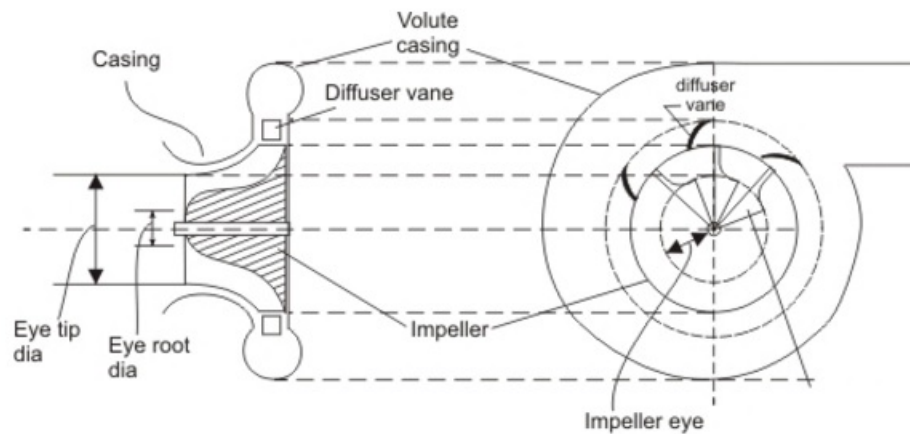


Figure 3.1: Components of a Centrifugal Compressor.

The most crucial design consideration for a centrifugal compressor is the impeller, the geometry of the vanes and the design of the volute scroll. Impellers can be categorized to three classes based on their exit blade angle  $\beta_{out}$ . When  $\beta_{out} = 90^\circ$  the impellers are called radial vane impellers. Impellers with  $\beta_{out} < 90^\circ$  are backward-curved or backward-swept vanes, while  $\beta_{out} > 90^\circ$  are called forward-curved or forward-swept. Based on the theoretical characteristics of these different classes of impellers their general head-flow characteristics are shown in Figure 3.2 and the characteristics are summarized in Table (3.1).

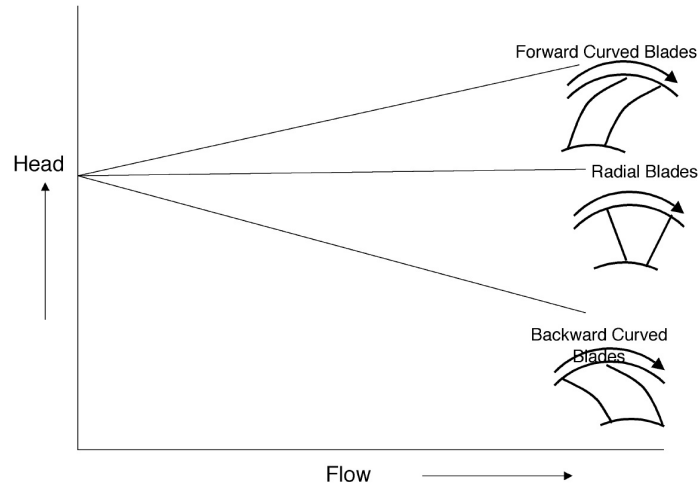


Figure 3.2: Head vs. flow relation of a centrifugal compressor [7].

Table 3.1: Advantages and disadvantages of different classes of impellers of a centrifugal compressor.

Class of Impeller	Advantages	Disadvantages
Radial Vanes	Reasonable compromise between low energy transfer and high outlet velocity.	Low pressure ratio.
Backward Curved Vanes	Low outlet kinetic energy. Wide surge margin. Low inlet Mach number.	Low energy transfer Complex stress on the vanes Complex manufacturing
Forward Curved Vanes	High energy transfer	High outlet kinetic energy. High inlet mach number. Complex stress on vanes. Complex manufacturing.

### 3.2.1 Dimensional Analysis of a Centrifugal Compressor

Dimensional analysis is a procedure, which represents physical situations that are grouped geometrically into dimensionless groups. A dimensional analysis approach is adopted to: (i) compare data from various types of machines; (ii) develop and design blade passages, blade profiles and diffusers with maximum efficiency and required pressure ratios; (iii) predict the performance of prototype units.

The important non-dimensional parameters for compressors are:

$$\begin{aligned} \text{Reynolds Number} \quad Re &= \frac{\rho DV}{\mu} \\ \text{Specific Speed} \quad N_s &= \frac{N\sqrt{Q}}{H^{3/4}} \\ \text{Specific Diameter} \quad D_s &= \frac{DH^{3/4}}{\sqrt{Q}} \\ \text{Flow Coefficient} \quad \phi &= \frac{H}{ND^3} \\ \text{Head Coefficient} \quad \psi &= \frac{H}{N^2D^2} \end{aligned} \quad (3.1)$$

The specific speed and diameter are used to select the type of compressors based on the compressor map. A generalized compressor map for compressor selection is shown in Figure 3.3. It is seen that high head and low flow require a positive displacement type compressor, while for a medium head and medium flow application a centrifugal compressor is used, while high flow and low head applications require an axial type compressor. The flow coefficient and pressure coefficient are used to determine various design characteristics. The generalized compressor map shows the effect of specific speed ( $N_s$ ) and specific diameter ( $D_s$ ). The most effective range of specific speed is between  $60 < N_s < 1,500$ , for a centrifugal compressor operation.

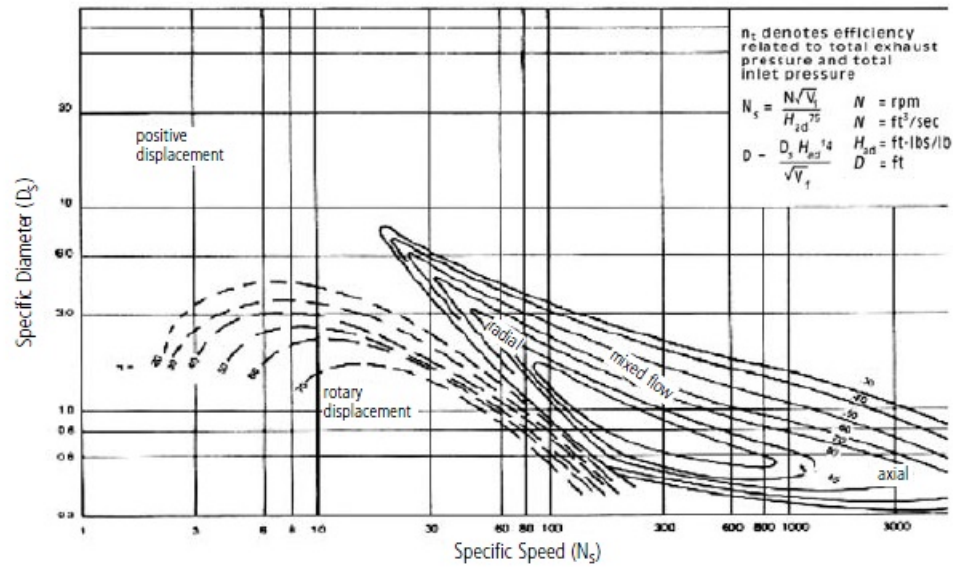


Figure 3.3: Generalized compressor map for compressor selection [7].

### 3.2.2 One Dimensional Flow Analysis

To design a centrifugal compressor impeller, the following performance characteristics must be defined:

- (i) Compressor total pressure.
- (ii) Inlet conditions (total pressure, mass flow and temperature).
- (iii) Adiabatic efficiency of the compressor.
- (iv) Exit conditions (total pressure, mass flow and temperature).
- (v) Properties of the operating fluid.
- (vi) Mass flow through the compressor.
- (vii) Operating conditions.

To numerically model the flow within the impeller, the flow can be modeled in two different planes, the meridional plane and the blade-to-blade plane. For the purpose of this research the hub-to-shroud model in the blade-blade plane approach is used. The method makes the assumption that all the stream tubes within the plane have the same mass flow,

the flow in each stream tube remains constant from the inlet to the exit. Thus, the mass flow through the stream lines can be expressed as:

$$\dot{m}/N = \int_{n_{in}}^{n_{out}} \int_0^{2\pi} \rho * W * (\cos\beta) * r d\theta dn \quad (3.2)$$

Assuming that at the inlet of the impeller the relative Mach number at the mean diameter is under 0.8. The relative Mach number is given by Equation (3.3).

$$M_{rin} = \frac{W_{in}}{a_{in}} \quad (3.3)$$

where,

$$a = \sqrt{\gamma g_c RT_{in}} \quad (3.4)$$

To estimate the absolute inlet velocity  $V_{in}$ , Equations (3.3) and (3.4) are used, where  $T_{in}$  is the inlet total temperature.

The inlet relative velocity  $W_{in}$  is presented in Equation (3.5)

$$W_{in} = M_{rin} * a_{in} = M_{rin} * \sqrt{\gamma g_c RT_{in}} \quad (3.5)$$

The blade angle at the inlet is estimated using Equation 3.6

$$V_{in} = W_{in} \cos(\beta_{in}) \quad (3.6)$$

From Equation (3.6) we derive:

$$T_{sin} = T_{in} - \frac{v_{in}^2}{2g_c J C_p} \quad (3.7)$$

Using Equations:(3.5)), (3.6), (3.7), we derive Equations (3.8) and (3.9).

$$V_{in} = W_{in} \cos(\beta_{in}) \quad (3.8)$$

$$U_{in} = W_{in} \sin(\beta_{in}) \quad (3.9)$$

The density at the inlet is given by the expression:

$$\rho_{in} = \frac{P_{sin}}{RT_{sin}} \quad (3.10)$$

Since the process between the static and total conditions is adiabatic, then the density at the inlet, Equation (3.10) can be re-written as:

$$\rho = \frac{P_{sin} \left( \frac{T_{sin}}{T_{sout}} \right)^{\left( \frac{\gamma}{\gamma-1} \right)}}{RT_{sin}} \quad (3.11)$$

The inlet flow-area can be computed and this from the cycle analysis, the mass flow rate is known from the continuity Equation (3.12).

$$\dot{m} = \rho_{in} A_{in} V_{m_{in}} \quad (3.12)$$

In Equation (3.12),  $V_{m_{in}}$  is the inlet meridional velocity at the inlet. If the prewhirl into the inlet is equal to the absolute inlet velocity, the mass flow through the compressor can be rewritten as:

Equation (3.12) is computed and then used to calculate the minimum hub diameter, so that the stress on the blades at the inlet is minimized.

Knowing the total pressure ratio as a design parameter can be expanded as,

$$\frac{P_{out}}{P_{in}} = \left[ \frac{\gamma_{in}}{\gamma RT_{in}} (U_{in} V_{\theta_{in}} - U_{out} V_{\theta_{out}}) + 1 \right]^{\frac{\gamma}{\gamma-1}} \quad (3.13)$$

Euler's turbine equation, the work input to the compressor for an axial flow with zero prewhirl angle can be expressed as:

$$U_{out} = \sqrt{\frac{\gamma RT_{in}}{\mu(\gamma-1)} \left( \frac{P_{out}}{P_{in}} \right)^{\left( \frac{\gamma-1}{\gamma} \right)}} \quad (3.14)$$

Where the outlet diameter  $D_{out}$  is expressed as:

$$D_{out} = \frac{U_{out}}{\pi N} \quad (3.15)$$

The adiabatic head can be derived from the Euler's turbine equation:

$$H_{ad} = c_p(T_{out} - T_{in}) = c_p\left(\left(\frac{P_{out}}{P_{in}}\right)^{\frac{\gamma-1}{\gamma}} - 1\right) = \frac{\gamma RT_{in}}{\gamma - 1} \left(\left(\frac{P_{out}}{P_{in}}\right)^{\frac{\gamma-1}{\gamma}} - 1\right) \quad (3.16)$$

The one dimensional analysis of the flow through the centrifugal compressor is useful for a primary design approach, but modeling, designing and predicting the exact flow through the compressor is complex. The methodology adopted to design and develop a centrifugal compressor with the scope of this research is presented next.

### 3.3 Design Methodology

In this section, a method of approach from design to implementation and testing of the ASU is presented.

The physics of the flow in a centrifugal compressor is complex and is highly dependent on the geometry of the impeller [30]. The parameters considered for the design of a centrifugal compressor can be categorized as follows:

- i. **Performance Parameters:** Mass flow rate values required for CC.
- ii. **Geometric Parameters:** The radius of the impeller at the inlet and outlet, the vane thickness, blade angles and axial length of the impeller.

- iii. **Operational Parameters:** The total inlet pressure, the air density and inlet temperature.

The performance characteristics required by the ASU for the efficient functioning of a CCW are defined by Kanistras et. al. in [23, 15, 34]. Kanistras et al. focuses on a comparative study and experimental investigation of CCW configurations in a low speed wind tunnel to determine the configuration that gives the best lift augmentation ratio. Different TE geometries ranging from blunt circular TE to dual radius hinged flaps are tested. The required mass flow for sufficient lift augmentation is determined to be different for the blunt circular TE and for the dual radius flap geometry based CCW. The relation between the mass flow of air and lift augmentation for each of these different configurations is quantified in these papers. The outcome of the these wind tunnel tests are used to define the performance characteristics of the ASU.

To supply the required mass flow to these different wing configurations two generations of Air Supply Units are presented. To facilitate the complex geometric design of each of the centrifugal compressor, a multi-stage optimization approach has been adopted, which can be summarized into the following four stages (Figure 3.4):

- i. **Stage I :** Preliminary design of different impeller configurations.
- ii. **Stage II :** Modification of impeller's geometry.
- iii. **Stage III :** CFD performance simulation.
- iv. **Stage IV :** Final design, Experimental validation and performance estimation of the compressor.

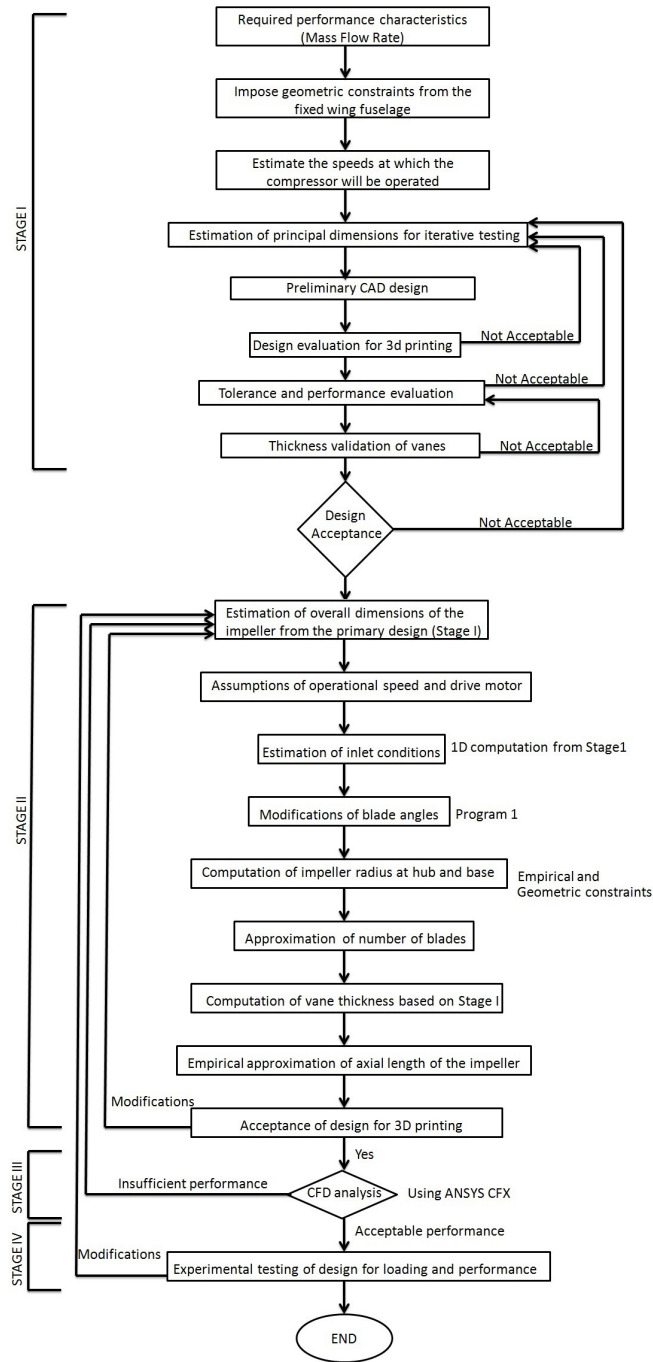


Figure 3.4: Design and experimental validation flowchart.

## Stage I

The maximum size of the ASU is geometrically constrained by the dimensions of the UAV's fuselage, where the ASU is mounted. The identified mounting area allows installations with  $D_h < 180$  mm and  $H_h < 150$  mm.

The rotational speed at which the ASU operates is defined by the brushless motor. Two motors, which are used to drive the different configurations of the ASU are, the EDF L2855 - 450 Watts motor for generation-1 and EDF L2855 - 900W for generation-2, capable of achieving a maximum RPM of 29,600. Impellers with forward vane configuration radial vane configuration and backward vane configuration, are designed with varying  $D_{in}$ ,  $\beta$  and  $h_{in}$  for each generation. Due to vane's load during compressor operation, the vanes require a minimum thickness ( $t_v$ ) of 0.8 mm to retain their shape and profile.

## Stage II

Stage I incorporated the constrained dimensions of the impeller, while Stage II focuses on deriving the dimensions, which lead to improved mass flow rates. To accomplish this, empirical data and the 1-D mass flow function are used.

The operational conditions at the inlet are estimated based on the geometry of the impeller at the inlet and the rotational speed:

$$U_{in} = r_{in} \cdot \omega_{in} \quad (3.17)$$

Equation (5.1) defines the tangential component of fluid's velocity. The value of  $r_1$  is approximated from Stage I as:

$$V = U \cdot \cot(\beta) \quad (3.18)$$

The absolute velocity at the inlet, which depends on the inlet blade angle:

$$a = \sqrt{\gamma \cdot g_c \cdot R \cdot T} \quad (3.19)$$

where:

$$W = M_r \cdot a = \frac{V}{\cos(\beta)} \quad (3.20)$$

From (3.20) the relative Mach number ( $M_r$ ) and the blade angle at the inlet  $\beta$  define the mass flow function. Since both parameters are interdependent, it is difficult to choose the most desirable values using computational methods, and a graphical approach is used. MATLAB<sup>®</sup> <sup>1</sup> is used to derive the non constrained parameters for the desired mass flow rate. Figure 3.5 shows the plot relating the mass flow function to the relative Mach number and the blade angle at the inlet for zero prewhirl angle.

The range for the relative Mach number at the inlet ( $M_r$ ) is computed based on the inlet radius of the impeller, which is a non-constraint dimension. Hence, a relation between the inlet and the outlet radius of the impeller is drawn using empirical data from [27] and [35]. An acceptable range for the ratio of  $R_{in}/R_{out}$  is determined to be from 0.3 to 0.7. Since the value of  $R_{out}$  is defined to be 70 mm, the range of relative Mach number can be estimated for the desired performance. The axial length of the impeller, the vane height at the output, the number of blades, the vane thickness and the hub diameter at the inlet are other parameters which affect the impeller's performance, which are modified based on the mass flow equation and empirical data.

The centrifugal compressors housing and its tolerance with the impeller are important parameters, which affect the performance of the ASU. The housing in the primary design is built with a large clearance, while the Version - II housing is built with a tolerance of 1

---

<sup>1</sup><http://www.mathworks.com/>

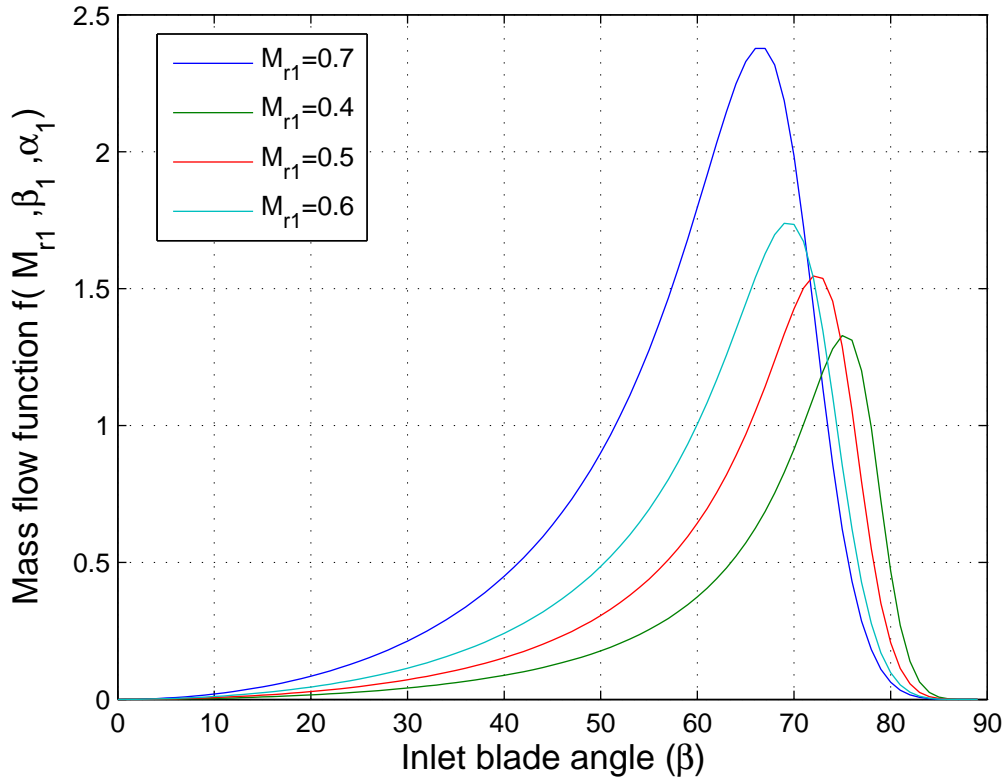


Figure 3.5: Numerical estimation of blade angle ( $\beta_1$ ) and Mach Number at the impeller inlet ( $M_{r1}$ ) at inlet using mass flow function at zero prewhirl angle.

mm with respect to the impeller to minimize clearance losses. Also an involute profile is retained but the height of the walls is kept within the tolerance limits of the impellers blade height at the outlet. The spline curve used to design the inlet for the compressor is derived from the blade curve of the impeller. The dimensions derived and calculated are then used in a direct design approach.

Section 3.4 goes through the different configurations of the ASU and various generations designed for their respective applications.

### **Stage III**

The design methodology in Stage I and Stage II, use a one-dimensional design approach and consist constraints with-in the design process. Due to the complex fluid flow through a centrifugal compressor, it is difficult to accurately estimate the performance of the design of each compressor just through theoretical analysis. CFD is used to bridge the gap between the theoretical design analysis and experimental result, thus aiding the design process to choose the ideal designs within the constrains. ANSYS CFX<sup>1</sup>, which is a commercial CFD program used to simulate fluid flow in a variety of applications, is used to simulate the ASU and estimate the performance at different RPMs. Further details of the analysis conducted is presented in this subsection.

The design geometries are generated and assembled in Solidworks and then exported into ANSYS workbench. To minimize complexity of the solving process the internal fluid domain of the housing is only used into which the impeller is inserted as an immersed solid. The computational domain is divided into two sub-domains namely the fluid domain which consists of the interior volume of the housing while the rotating solid is the impeller itself. The boundary conditions of the fluid domain of the compressor are set to atmospheric pressure. The rotation of the impeller is defined with respect to the rotating axis of the impeller defined prior to importing the geometry to ANSYS CFX. The CFD tool is used to simulate the flow within the ASU at multiple steps ranging from the minimum to the maximum RPMs achievable by the respective motors for each generation.

The results from the CFD tool are presented along with the experimental results in Section 3.5.3.

---

<sup>1</sup><http://www.ansys.com/Products/Simulation+Technology/Fluid+Dynamics>

## Stage IV

The experimental testing phase for the ASU consists of the following steps.

- i. The compressor is tested at various RPMs. The velocity at the outlet of the compressor is recorded at different RPMs. The results are used to establish the speed-mass flow relationship for each compressor configuration.
- ii. The ASU integrated with the framework, which consists of the ADS and CCW structure, is tested to quantify the performance in terms of the jet velocity.
- iii. The final performance of the ASU is tested on-board the UC<sup>2</sup>AV, while being operated by the controller.

## 3.4 Model(s) Description

### 3.4.1 Generation-I

The primary function of the ASU is to supply the required mass flow of air to the CCW on-board the UC<sup>2</sup>AV. Kanistras et. al. [34] defines the required mass flow to achieve effective lift augmentation in different CCW configurations. Nine preliminary configurations of impellers and three configurations of housings are categorized into the first generation of the ASU. Each of these designs vary with respect to their geometric parameters. All the configurations are designed and are computationally and experimentally tested to validate the geometry-performance relations. Each impeller configuration is tested for the best fit geometric parameters, which would be incorporated in the final design. The 3 different housings are tested to ideally match the impeller's shape at the intake and exit . Also the design of the housing is modified to accommodate for the motor mount to increase the

efficiency of the compressor. Figure 3.6 shows 9 different configurations along with their performance.

Centrifugal Compressor Version	Picture	Centrifugal Compressor Configuration								Centrifugal Compressor		
		Impeller Type	Vane Profile	Impeller Radius (mm)	Outlet Radius (mm)	Housing	Inlet Vane Angle (degrees)	Outlet Vane Angle (degrees)	Diffuser	Max RPM	Max outlet velocity (m/s)	Mass Flow Rate (kg/s)
Version-I		Backward Vane	Straight	50	4	Housing I	60	60	YES	24900	35.2	0.00173308
Version-II		Backward Vane	Splined	60	5	Housing II	50	70	N/A	23866	48.42	0.00372495
Version-III		Forward Vane	Splined	60	5	Housing II	50	70	N/A	23566	52.03	0.00400267
Version-IV		Backward Vane	Straight	60	5	Housing II	60	60	N/A	24116	49.4	0.00380034
Version-V		Forward Vane	Straight	60	5	Housing II	60	60	N/A	23910	53.7	0.00413114
Version-VI		Backward Vane	Straight	70	5	Housing II	60	60	N/A	23500	63.05	0.00485044
Version-VII		Forward Vane	Straight	70	5	Housing II	60	60	N/A	22650	61.29	0.00471504
<b>OPTIMIZATION</b>												
Version-VIII		Backward Vane	Straight	70	5	Housing III	72	62	N/A	22833	70.46	0.00542049
Version-IX		Forward Vane	Straight	70	5	Housing III	72	62	N/A	22833	69.9	0.00537741

Figure 3.6: Different impeller configurations of generation-I ASU.

Version I through VII of the impeller designs are base-line designs with conventional simplistic vane geometries. All these configurations are designed to vary in one geometric parameter with respect to the next or prior configuration in the sequence. Analysis of experimental results show that the 3D printed models operate at different mass flow and

Housing Name	Housing 1	Housing 2	Housing 3
Picture			

Figure 3.7: Different housing designs generation-I ASU.

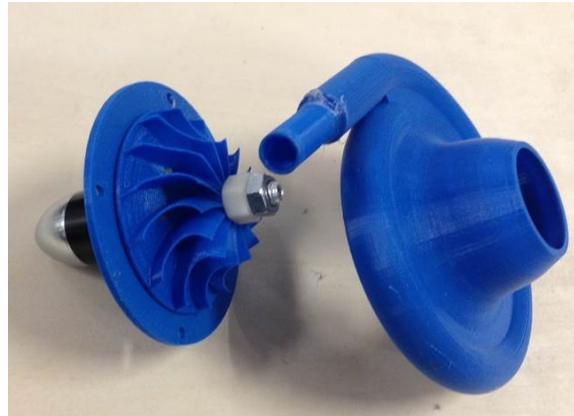


Figure 3.8: Assembly of the generation-I ASU.

pressures compared to the estimated performance during the theoretical design. Thus a stage based optimization was conducted to bridge the theoretical design and experimental models. As a result the Version VIII and IX show better performance compared to the prior designs. The post optimized designs have splined vanes and varying geometry from the inlet to the outlet. Although these configurations performed closer to the required mass flow conditions, the pressure ratio that the compressor could achieve was still low, and as a result considerable losses and back flow was observed at the inlet of the compressor.

### 3.4.2 Generation-II

Kanistras et al. [9] deduces that dual radius flaps used for CC applications needs a mass flow of 0.0288kg/s, which was set as the performance parameter during the design process of the ASU for the UC<sup>2</sup>AV. The design is carried out using the design methodology,

and additionally the best fit geometric parameters through the analysis of the generation-I compressors. Since the backward vane impeller with an forward vane inducer section showed the best performance in the Generation-I of the ASU, the second generation ASU retained this characteristic. The experimental testing showed that there was back flow and losses in the Generation-I ASU, hence a shrouded impeller design was used in the second generation, to minimize the losses between the housing and the impeller. To improve the performance of the ASU with respect to the pressure ratio, an expanding volute based housing was designed. Additionally the constraints on the CCWs and UC<sup>2</sup>AV are incorporated into the design. The design of the ASU is shown in Figure-3.10 .

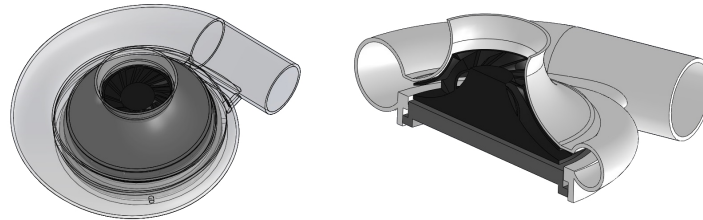


Figure 3.9: CAD design of the generation-II ASU.



Figure 3.10: Various components of the generation-II ASU.

### 3.5 Performance characterization

This section describes the characterization of performance curves for the ASU. The performance is presented as a relation of  $V_{out}$  and RPM, and a comparative analysis between CFD and experimental results is presented. The ASU is a variable displacement centrifugal compressor capable of functioning with various CCWs. It is essential to experimentally validate and quantify the performance of the compressor over a wide range of operation (RPM, Q,  $P_r$ ). A compressor's performance is measured as a relation between the flow rate and pressure ratio. A commonly used approach to represent this relation is in the form of performance curves for different RPMs [ref]. The relation between Q vs  $P_r$  that characterizes a centrifugal compressor performance is shown in Figure 3.11.

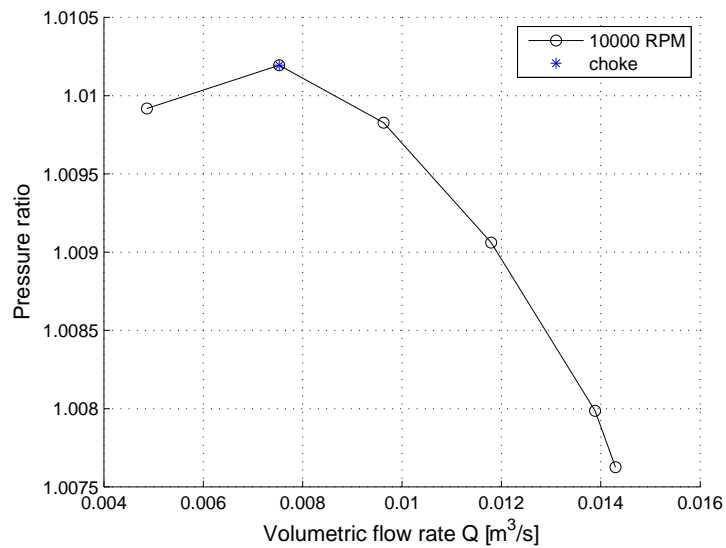


Figure 3.11: Performance curve of the ASU at 10,000 RPM.

### 3.5.1 Instrumentation

#### Pitot Probe

Air speed at the outlet of the centrifugal compressor is an important parameter during testing. To measure the velocity at the outlet ( $V_{out}$ ) with accuracy, a pitot tube (Figure 3.12) is modified and calibrated. A conventional pitot tube is selected and the inner probe diameter is modified. The probe length is extended and the inner/outer diameter is gradually reduced, using brass tubing. The outer diameter of the probe is then measured to be 0.5 mm with an inner diameter of 0.3 mm. The pitot probe is connected to a MPXV5004 differential pressure sensor, which provides an analog voltage as the output. The volumetric flow rate ( $Q$ ) at the outlet of the ASU is calculated using Equation (3.21).

$$Q = V_{out}A_{out} \quad (3.21)$$

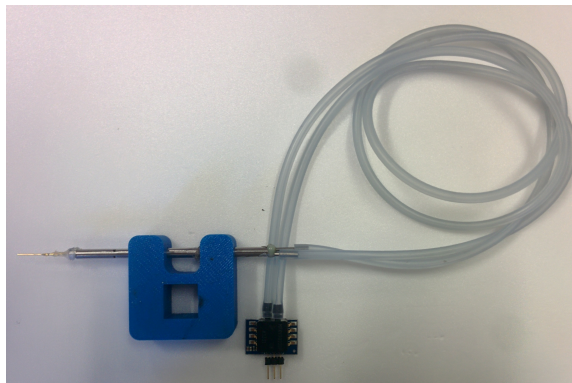


Figure 3.12: Calibrated pitot probe with an inner diameter of 0.3 mm.

## Pressure sensor

To measure pressure at the inlet and outlet of the compressor a Freescale semiconductor MPXV5004 series transducer is used. The sensor combines a strain gauge implants with thin-film metalization, and bipolar processing to provide an accurate analog output signal which is proportional to the applied pressure. The pressure sensor is calibrated using the static pressure of a wind tunnel running at various speeds. The analog voltages from the sensor are mapped to the ambient static pressure measured by the manometer. The pressure sensor is connected to an averaging static pressure tap to measure the static pressure at the inlet and the outlet of the ASU.

## RPM measurement

To measure the RPM values of the centrifugal compressor motor, a Hall effect sensor reads the changing magnetic flux from the permanent magnet mounted into the housing of the motor (Figure 3.13). To control the brushless motor, a Hitec servo programmer and an Arduino micro-controller based PID speed controller is used.



Figure 3.13: Left: The airspeed sensor (pitot tube). Center: The Hitec servo programmer and controller. Right: The Hall effect sensor. <sup>2</sup>

## Temperature sensors

Thermocouples, which are temperature measurement transducers, are commonly used for compressor testing. National Instruments provides low-cost ready-made thermocouples

for accurate temperature measurement purposes. The thermocouples are readily integrable to an Analog to Digital (A/D) converter, which is calibrated to display the measured temperature. The sensor's resolution is  $0.1^{\circ}\text{C}$  with a range from 0 to  $500^{\circ}\text{C}$ . These sensors are used to measure temperature of the fluid at the inlet and the outlet of the ASU.

### 3.5.2 Experimental Setup

The test measurements, the location of the instrumentation and the testing procedures to accurately evaluate the performance of the compressor follows the guidelines in AMSE Performance Testing Code (PTC) 10. The schematic of the test system is shown in Figure 3.14.

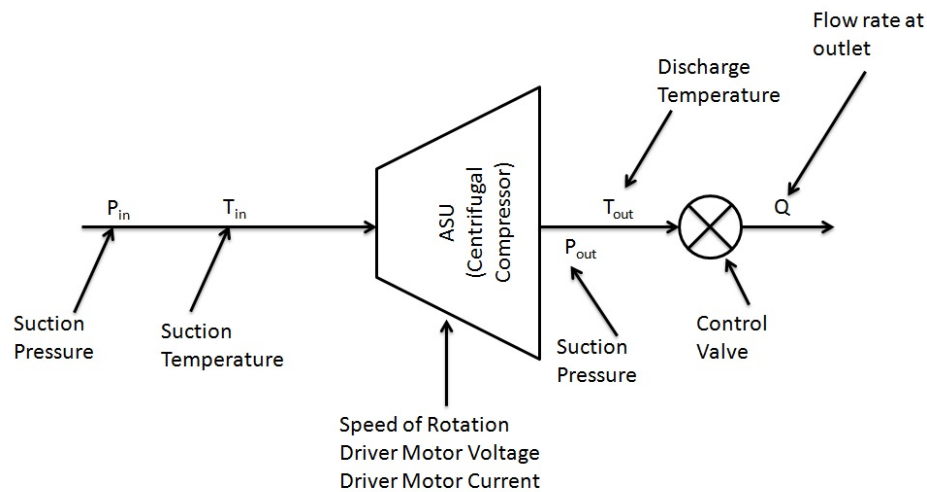


Figure 3.14: Schematic of the location of the sensors.

To evaluate the performance parameters as prescribed by AMSE PTC 10 the necessary experimental measurements can be summarized as:

- Temperature at the inlet
- Pressure at the inlet

- Temperature at the outlet
- Pressure at the outlet
- Flow rate through the compressor
- Speed of rotation
- Compressor dimensions

AMSE PTC 10 also describes the location of necessary instrumentation for testing of the compressor. The experimental setup and performance characterization of the ASU is conducted based on experimental testing layout shown in Figure 3.14.

The rotational speed at which the ASU operates is defined by the brushless motor (EDF L2855 with a power rating of 900 Watts, maximum RPM of 29,600 at no load), which drives the impeller. The Electronics Speed Controller (ESC) is used to power the motor. The RPM sensor is connected to the ESC and the motor to record the speed of the motor (N). The power consumed by the motor and the ASU, is recorded as electrical power in terms of voltage (V) and current (I) draw from the battery.

To simulate the circulation control system, air enters the ASU through a suction-end (an extension from the inlet of the impeller to the exterior of the UAV) and is discharged through the extended outlet. At the inlet-end of the ASU, 4 static pressure taps are located close to the impeller. An averaging pressure tap connects the 4 taps to a calibrated pressure transducer, which reads ambient static pressure at the inlet ( $P_{S_{in}}$ ). A thermocouple probe at the inlet measures the temperature ( $T_{in}$ ). At the outlet of the ASU prior to the discharge a similar set of pressure taps and temperature sensors are located to measure the pressure ( $P_{S_{out}}$ ) and temperature ( $T_{out}$ ). The calibrated pitot probe sensor is used to record air velocity at the outlet of the centrifugal compressor. The pitot probe, which is placed at the exit of the outlet, can be freely moved across the outlet while retaining the same height

(at the middle of the circular exit) and distance from the exit. Three points at the exit across the circular exit are recorded at different RPM. A control valve located at the outlet is used to control the flow rate through the system. The CAD model of the testbed and the location of the sensors is shown in Figure 3.15.

The test unit consists of the ASU and the physical probes and actuators integrated to measure the test parameters. The test setup also consists of a control unit and Arduino/LABVIEW based data acquisition system. The control unit runs a tunable gain PID control on the motor to regulate the speed of the motor accurately. The speed from the ESC, the analog values of the pitot, the pressure transducers and the voltage/current sensors are recorded by the micro-controller, which communicates over a USB serial port to the LABVIEW control code. The control unit uses calibration codes from the sensors to convert the analog voltages to the respective physical measurements. The schematic of the control unit is shown in Figure 3.16.

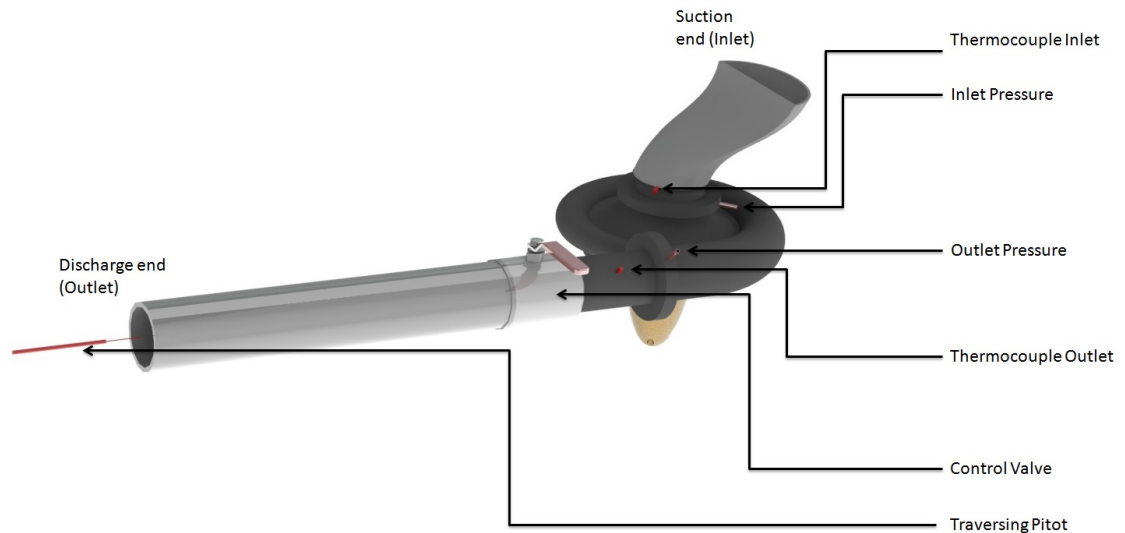


Figure 3.15: The experimental setup of the ASU.

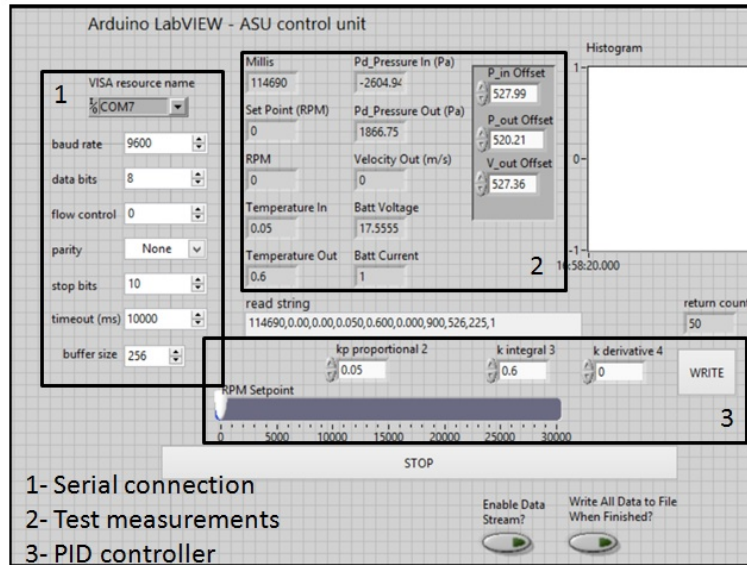


Figure 3.16: The controller unit for the ASU.

### 3.5.3 Experimental Testing

The pitot probe is used to collect data at three points along the exit of the ASU. The points are equally distanced and at the same height (at the middle of the circular exit). Data are collected from 10000 to 26000 RPM with increments of 4000 RPM. Although the motor can achieve up-to 29000 RPM (it is the maximum that the motor can operate at the given loading), this point is not tested to maintain a margin of safety of the test unit. The tests are conducted by regulating the set-point of the PID controller. Data are recorded (100 readings) from all the test sensors, once the motor achieves a steady state velocity. The samples are averaged and the results are displayed on the control unit. The test is continued by changing the value position between predefined increments to regulate the flow rate through the ASU.

At a given RPM as the flow rate decreases through the ASU it reaches a critical point, at which the flow separates from the impeller. Flow separation causes changes in the fluid velocity and direction resulting in unsteady flow. This point of operation is known as the

surge or choke point. The Surge point is the lower limit of flow for stable compressor performance. This is characterized in experimental testing by a drop in pressure ratios with reduction in flow using the control values. It is observed that the surge is prominent at higher RPMs, where at higher flow rate conditions occur. As the flow rate reduces, the pressure ratio increases, thereby characterizing the ASU. The test are conducted on three different days and the average data of the runs are presented. Figure 3.17 shows the performance curves for the ASU as a relation between the average flow rate and the average pressure ratio.

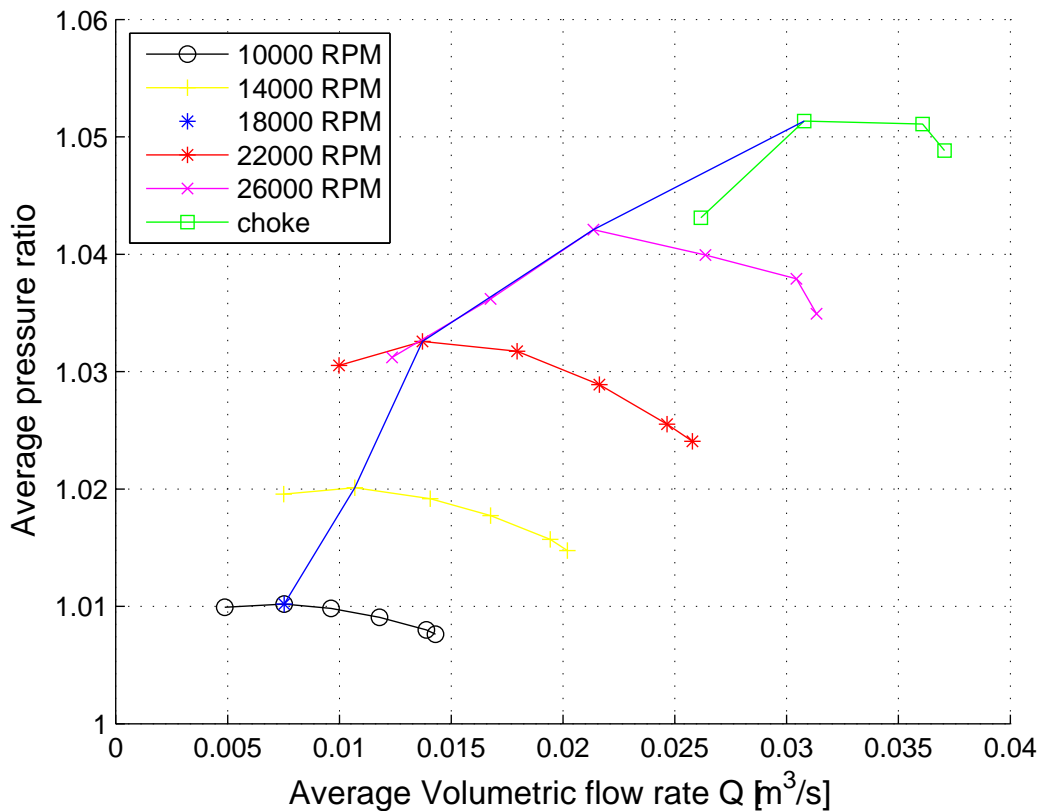


Figure 3.17: Compressor map of the ASU.

The plot in Figure 3.18 shows the deviation of the velocity at each point from the average line (shown in black) at each RPM value along the outlet of the ASU. It is shown

that the flow is not fully developed since the ASU exit is close to the housing. At all tested RPM the velocity data follows the same trend. However, the maximum variation of 3 m/s from the mean velocity is seen on the first data point. This performance is expected due to the rotation of the flow inside the compressor. It is important to calculate the average velocity of the outlet of the compressor, to minimize errors in the volumetric flow rate computation. Figure 3.19 shows the average velocity at the ASU outlet at each RPM. A linear correlation, as expected, between the average velocity and the RPM is recorded. To validate the experimental results, a CFD analysis is performed using ANSYS CFX. Tetrahedral mesh elements with fine smoothing and 0.7 mm element sizes are used for the complex geometry of the ASU. Transient state simulations are conducted and the results of the ASU at discharge are recorded. The mean values of the velocity at the outlet are in close agreement with the experimental results (Figure 3.19).

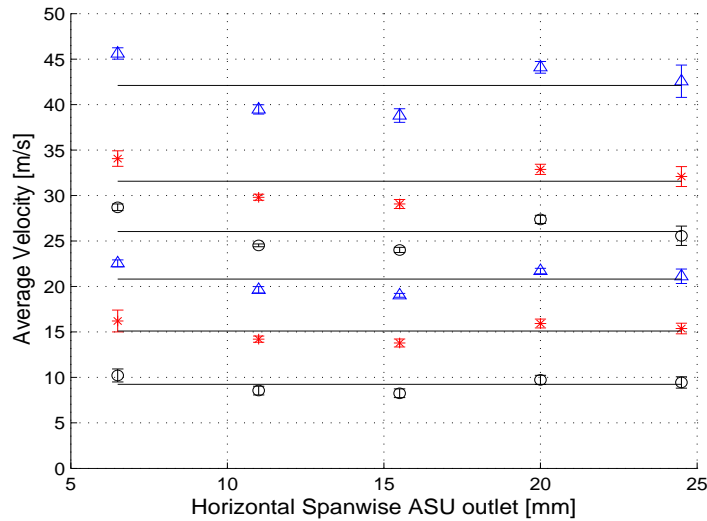


Figure 3.18: Velocity distribution at the ASU outlet.

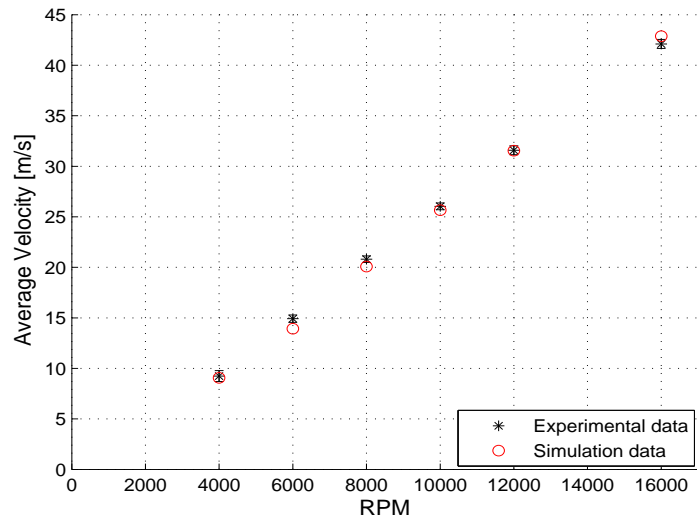


Figure 3.19: Experimental and simulation data of the ASU performance at different RPM.

# Chapter 4

## Circulation Control System Integration

The pneumatic system to support CC on-board the UC<sup>2</sup>AV consists of multiple sub-components, which are essential to achieve efficient CC. Although the ASU (pneumatic source) is the most significant component, a pneumatic system to deliver the mass flow air to the TE with minimized losses, is also an important part of the overall system. The Air Delivery System (ADS) is a pneumatic system capable of handling high pressures and mass flow, to deliver a continuous supply of air to the slot. The system is designed to provide a mass flow of 0.03 kg/s and distribute it equally between two flow paths to either side of the wing. The ADS consists of: i) the intake ducting passage of the ASU; ii) the internal pneumatic junction and tubing that connects the ASU with the plenum; and iii) the plenum, which is a vaned, straight-walled wide angle diffuser, responsible for delivering the required mass flow uniformly along the span. A block diagram of the CC system is shown in Figure 4.1. This chapter describes the analysis of the ADS system components and their integration with the ASU to deliver a high energy jet at the TE of the CCW.

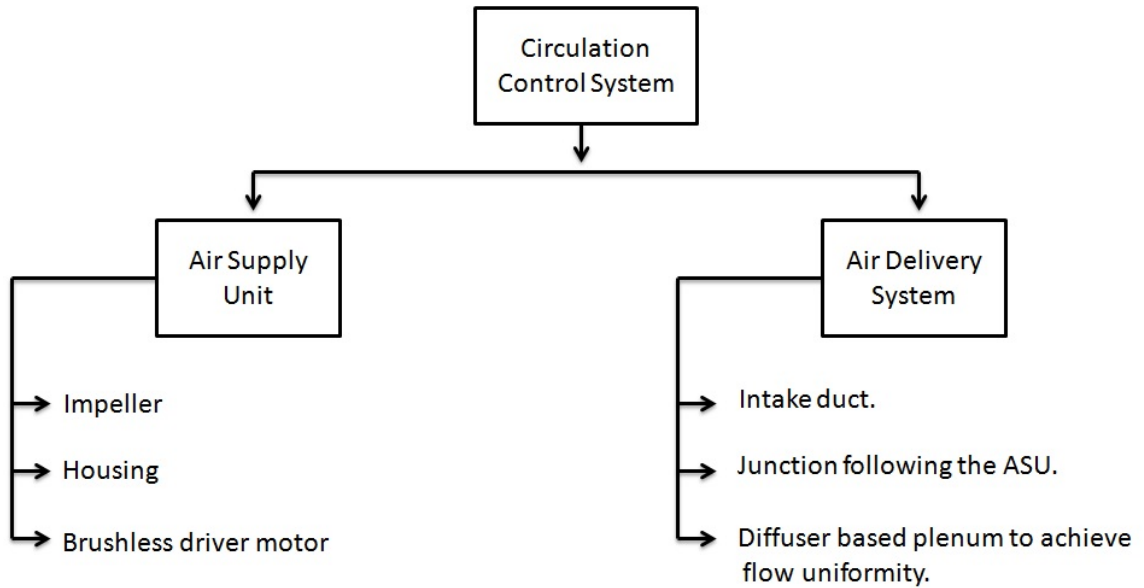


Figure 4.1: Schematic representation of the Circulation Control System.

## 4.1 Intake Duct Design

The ASU is located in the fuselage along the center of gravity of the UAV. The precise location is selected to minimize the inertial torques when the ASU rotates. The inlet of the ASU causes undesired suction where the sensors and other peripheral devices are located. This suction in the fuselage creates a low pressure region, which can lead to structural damage and introduce errors to the instrumentation. To eliminate this, an intake duct is designed to transfer the suction end of the ASU in the underside of the fuselage. The intake duct is also responsible for moving the free-stream velocity to the inlet while eliminating an undesired pre-whirl in the flow which deteriorates the ASU performance. An iterative design approach based on the a CFD flow field analysis is adopted to find the best design. The design of the duct is constrained in the longitudinal distance (X) due to the location of the ASU and the instrumentation. The design of the duct and the location of the ASU are shown in Figure 4.2.

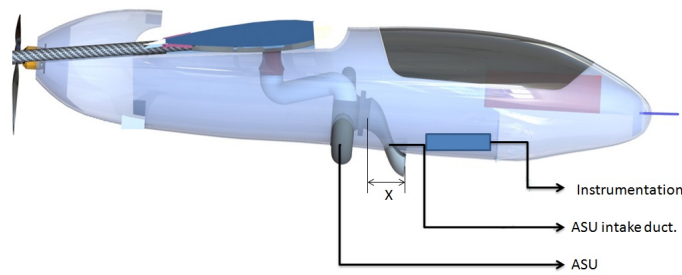


Figure 4.2: CAD design integration of the fuselage, the ASU and the intake duct.

A flow field analysis of the duct is conducted using ANSYS Fluent. A complete 3-D analysis is performed for different inlet velocities to simulate flight scenarios. A tetrahedral mesh with a maximum cell size of 0.5 mm is used to ensure accuracy in results based of a mesh validation study. A pressure-based, steady state analysis is performed using the K-e viscous model. Inlet boundary condition is set to a velocity inlet type and outflow boundaries are used. The intake duct is evaluated at 4 different inlet velocities from 5 to 20 m/s, simulating different stages of flight. Flow field analysis is presented in Figure 4.3. Regions of stall are observed within the flow field, however the design is only evaluated for possible prewhirl of the inlet flow.

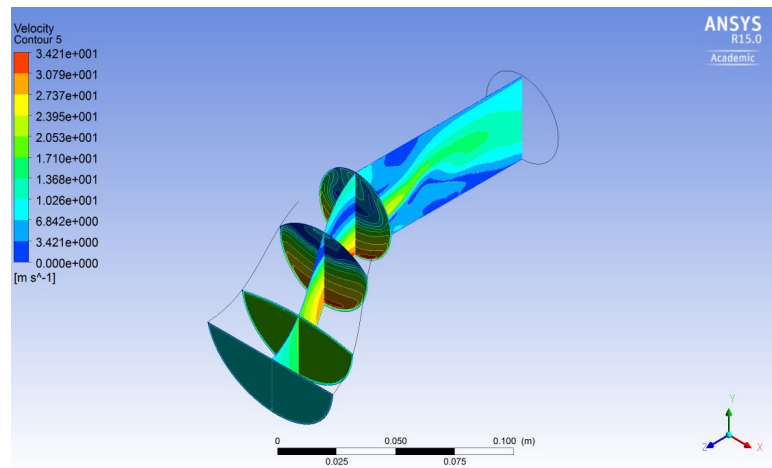


Figure 4.3: Contours of the flow field in the intake duct at 10 m/s inlet velocity.

## 4.2 Junction Design and Analysis

Chapter 3 presents the details of the performance of the ASU, which acts as the pneumatic source for the CC system. It is observed that the pressure head created at the outlet of the ASU plays an important role in achieving efficiency/performance. The immediate component, downstream of the ASU is a junction that connects the outlet of the ASU to the pneumatic tubing within the wings. The pressure head and losses created by this junction change the flow rate through the compressor and result in reduced CC efficiency. Losses in a pneumatic system can typically be categorized as major and minor losses [36, 37]. The total head losses created within a pneumatic system is expressed as:

$$\Delta P_L = \Sigma \frac{4f_{in}L_{in}\rho}{D_{in}} \frac{V_{in}^2}{2} + \Sigma K_i \frac{\rho V_{in}^2}{2} + \Sigma \Delta P_{comp} \quad (4.1)$$

At the junction, where the fluid displacement is small, minor losses in the system are dominant. Since the flow in the junction is dominated by minor losses, using the loss coefficient method [8], the K factor is calculated as follows:

$$K = \frac{\Delta P}{\frac{1}{2}\rho V^2} \quad (4.2)$$

Values of simple constant K factors, which depend on specific geometric details, have been determined experimentally for many configurations of bends, fittings, valves etc. and can be found in [38, 39]. However, the junctions used on the ADS are designed based on space and weight limitations with different geometries compared to standard junctions. Thus, the K factor for each junction that is used and the head losses are determined using CFD analysis. For that purpose, four junctions are designed (Figure 4.4) and flow analysis using ANSYS Fluent is conducted to determine the design with the minimum head losses.

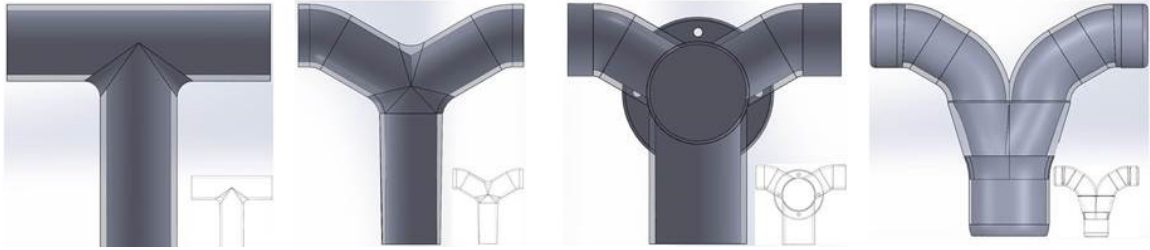


Figure 4.4: CAD designs of junction configurations [8].

## Junction Performance

The performance of the four junctions is analyzed using ANSYS Fluent and a complete 3-D analysis is performed for each case. A tetrahedral mesh with a maximum cell size of 1 mm is used to ensure accuracy in results after a mesh validation study. A pressure based, steady state analysis is carried out using a K- $\epsilon$  viscous model. The inlet boundary condition is set to a velocity inlet type, and the junctions are evaluated at 5 different inlet velocities from 10 to 50 m/s, which correspond to the complete range of operation of the system. To calculate the K factor using Equation (4.2), the pressure drop and the outlet velocity are recorded along with the flow field in each case.

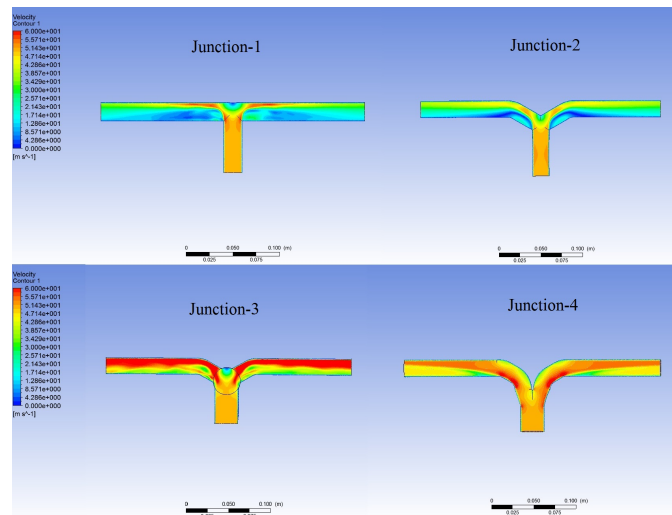


Figure 4.5: Velocity contour of the junctions at 50 m/s inlet velocity from CFD analysis[8].

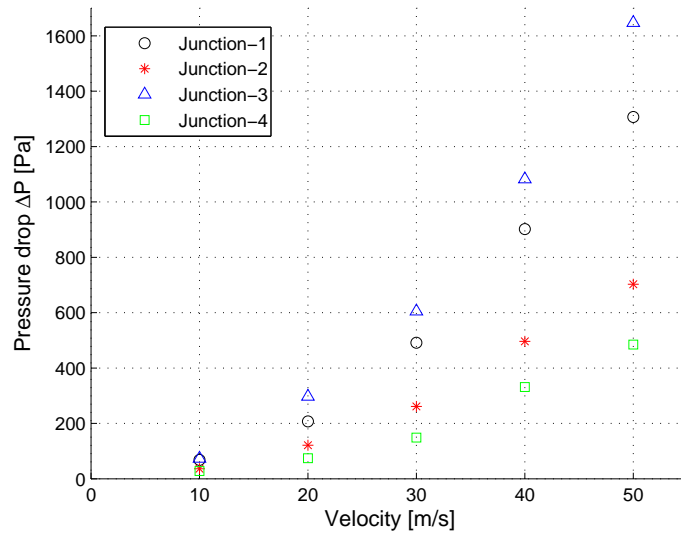


Figure 4.6: CFD analysis on the four junction designs. The recorded pressure drop for different velocities is presented [8].

The plot in Figure 4.6 shows the pressure drop in each of the configurations at various inlet velocities. It is observed that due to a change in cross sectional area the fluid in Junctions 1 and 2 have a lower velocity at the outlet. On further flow field analysis presented in Figure 4.5, the creation of a large stagnation point in Junction-1 and a smaller yet prevalent stagnation point in Junction-2 adds to the losses in these two designs. Although Junction-3 and Junction-4 perform better in terms of the outlet velocity, Junction-3 has a large pressure drop and an unsteady flow field due to the reservoir shown in Figure 4.4. Table 4.1 shows the average K factor value for each of the junctions over the range of inlet velocities. The low K factor, the stable flow field and minimal pressure losses, qualifies Junction-4 for experimental evaluation.

Table 4.1: K factors for the four junctions at different inlet velocities.

<i>Velocity (m/s)</i>	<i>J-1</i>	<i>J-2</i>	<i>J-3</i>	<i>J-4</i>
10	1.39	0.74	1.50	0.57
20	1.06	0.62	1.52	0.38
30	1.11	0.59	1.37	0.34
40	1.15	0.63	1.38	0.42
50	1.07	0.57	1.34	0.40

### 4.3 Plenum Design and Analysis

An important factor for the efficiency of CC and stability of the CC based UAV is the flow uniformity at the slot. This section presents the design to achieve flow uniformity evenly across the span. Plenum designs for CCWs have been investigated in the past, and several techniques (metal foam treatment, perforated plates, metal barriers, Rigimesh material etc.) to tackle this problem and to achieve flow uniformity at the slot-exit along the span have been tested [40, 41]. However, in smaller scale wings the internal-plenum design is dictated by space constraints, adding complexity to the design. A preliminary investigation showed that a diffuser-based plenum could provide the necessary jet at the slot. The challenge to use a diffuser-based design in the plenum is the deceleration of flow and stall regions in the fluid between walls. These regions of stall disrupt the uniformity, which must be compensated by placing adequate vanes in the diffuser. The vanes divide the diffuser into a series of sub-diffusing passages with area ratios and divergence angles smaller than the initial diffuser. That way, stall is avoided and each passage can operate at near optimum pressure recovery. The deceleration of flow must be compensated by a nozzle to achieve high velocity jets at the nozzle end (slot) of the plenum.

A vaned straight-walled wide angle diffuser with a nozzle at the exit to provide flow uniformity across the span of the wing is used. The diffuser is divided using nine equally distanced vanes as Figure 4.7 demonstrates. The skin of the wing above the slot has a thickness of 0.35 mm and without any internal support, the slot will deform and increase during blowing. To prevent this, nine equally distanced stationary aerodynamic standoffs are designed into the aft plenum along the span to maintain a known slot height. Before the air is driven through the diffuser, it passes through an elbow tube fitting, which results to a non-uniform flow across the outlet of the tube. To correct the direction of the flow, three vanes are placed inside the tube and ANSYS Fluent CFD analysis is conducted to find the exact position that the vanes should be placed. The design showing the best result is 3-D printed and attached to the plenum as Figure 4.7 illustrates. Further details of the design a can be found in [9].

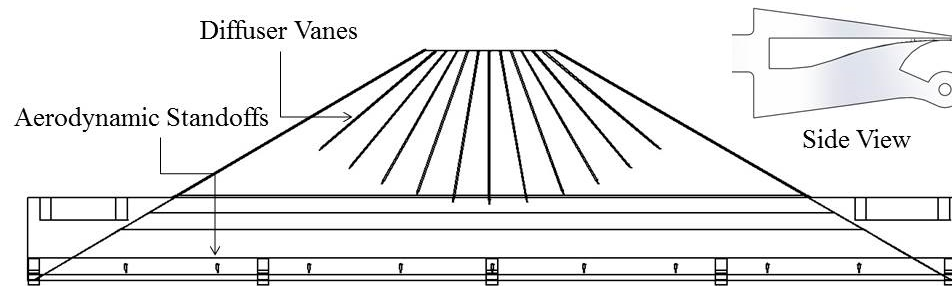


Figure 4.7: Plenum CAD design: The vanes at the inlet are for flow correction and the vanes in the diffuser achieve uniformity. Nine standoffs are placed to avoid slot deformation during plenum pressurization[9].

## Plenum Performance

For flow uniformity testing, a pitot probe is used to measure the velocities at the jet ( $V_{jet}$ ) across the span (the pitot tube can move freely with equal increments across the span while retaining the same height and distance from the slot). Measurements are recorded at 20 points and the process is repeated 6 times for each inlet velocity. For these experiments,

air is supplied to the inlet of the plenum using a stationary compressor. The average of the 6 runs for each inlet velocity along with the mean velocity (shown in black) at each case are shown in Figure 4.8. Flow uniformity is tested at 5 different inlet pressures 25 kPa, 50 kPa, 75 kPa, 100 kPa and 200 kPa. The results showed that even at velocities higher than the operating range the plenum responds well and despite the losses, flow uniformity is achieved.

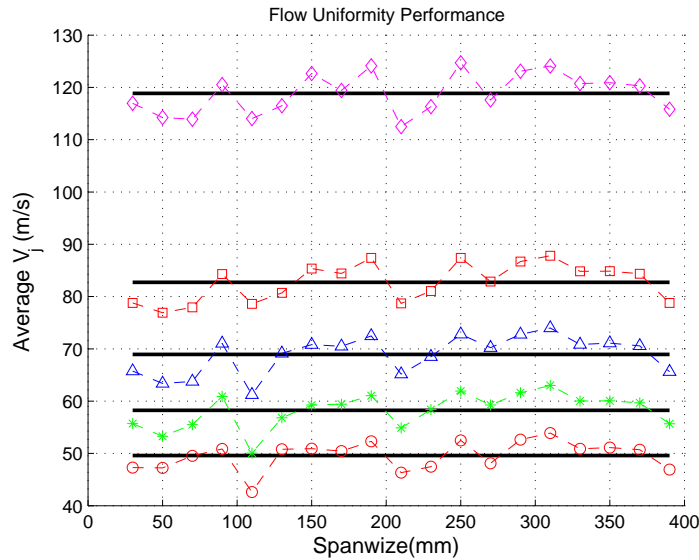


Figure 4.8: Flow uniformity performance across the span of the wing[9].

## 4.4 CC System Integration

The CC system integrates the ASU, the inlet ducting passage, the junction, pneumatic tubing and two diffuser based plena which distribute the air evenly across the slot. A CAD model of the CC system is shown in Figure 4.9. The ASU is the pneumatic power source for this system. As the ASU rotates, air is sucked from the inlet of the duct from the exterior of the fuselage. The kinetic energy and static pressure of the air increases as it moves through the ASU. The junction following the ASU connects the two plena (located on either side

of the wing) to the outlet of the ASU. The impeller of the ASU rotates at different RPM, and thereby different jet velocities at the slot are achieved. This section characterizes the system, based on the RPM of the ASU and the jet velocities achieved are used to estimate the  $C_{\mu}$ .



Figure 4.9: CAD model of the CC system [8].

## CC System Performance

An experimental evaluation of the overall system is conducted by testing the systems performance at different RPM. The experimental setup of the CC system is presented in Figure 4.10. the setup consists of dual radius flaps integrated to the plena to form the slot . The distance between the two plena (500 mm) is based of the final location of the system on the UAV. The ASU is located under the ADS to simulate its position inside the fuselage and at the center of gravity of the aircraft. The pitot probe is positioned on the slot exit to measure the velocity at the jet ( $V_{jet}$ ) across the span (bottom right Figure 4.10). It can be moved freely across the span while retaining the same height and distance from the slot. Measurements are recorded at twelve points spaced equally across the span.



Figure 4.10: The experimental setup of the CC system.

The flow uniformity across the span is evaluated along with the repeatability of the system. The plot in Figure 4.11 presents the performance of each plenum and the deviation of the velocity from the average line (shown in black) at each RPM is shown. The experimental procedure is repeated five times for three different RPM values since high flow uniformity performance and repeatability before the system is ready to be integrated on-board the UC<sup>2</sup>AV is required. As Figure 4.11 demonstrates, only in one point (on the left side of the wing at the higher RPM) the required performance is not achieved. A slight deviation in jet velocities is observed on one side of the system. To investigate the design a CFD analysis is conducted, to visualize the flow field. A volume rendering of the velocity field results is presented in Figure 4.12. After validation through CFD analysis, it is concluded that the deviation in velocity was a result of the deviation in the slot height, caused by fabrication error. A change in flap design was suggested to rectify this and is adopted on-board the UC<sup>2</sup>AV.

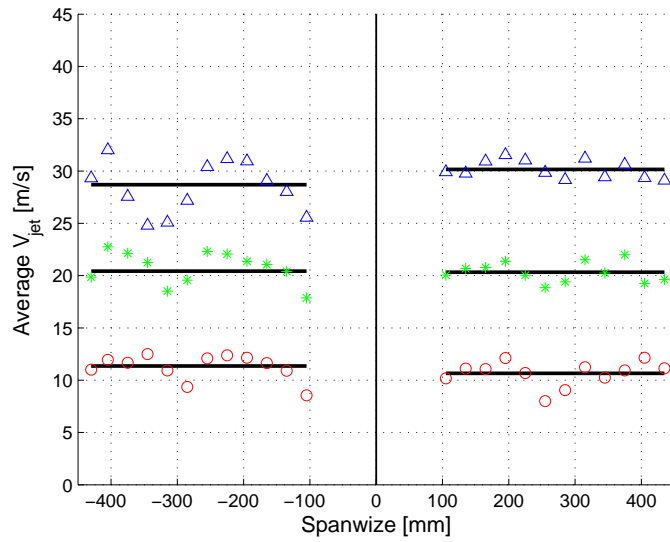


Figure 4.11: Experimental results representing the performance of the  $V_{jet}$  at the slot across the span on each plenum for different RPM values. The deviation of the  $V_{jet}$  from the average line (shown in black) at each RPM value is shown.

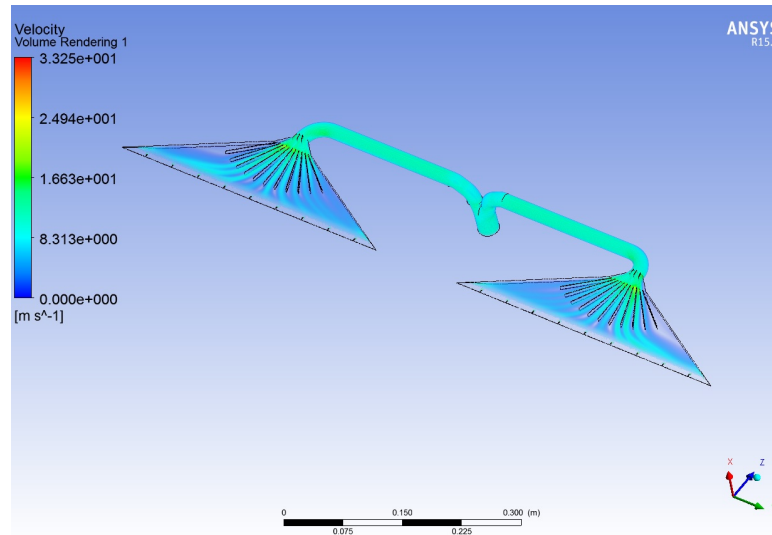


Figure 4.12: CFD analysis of the plenum designs.

The power consumption (in terms of the voltage and current draw from the battery) and the flow rate through the system (in terms of  $V_{jet}$ ) are recorded. Using the compressor map of the ASU shown in Section 3.5.3, the system's current performance is compared to the

estimated operating condition. The  $C_{\mu}$  based on the  $V_{jet}$  and an average flight velocity is computed, which is used to compute the estimate the lift augmentation.

## ASU Working Region Characterization

The ASU and its performance has been characterized in Chapter 3. Since the performance curves for the ASU are spread over a range of pressure ratios and flow rates for each RPM, the working region of the ASU and framework needs to be characterized. The power consumption of the ASU is used to establish the working region. Figure 4.13 shows the working region of the ASU.

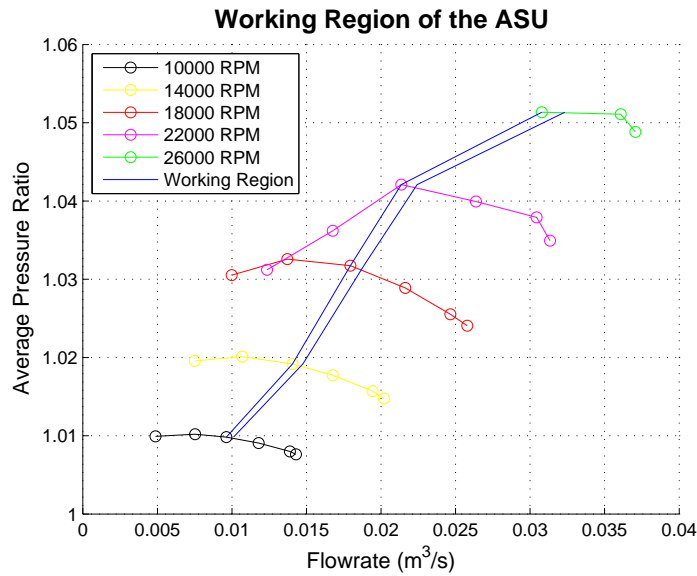


Figure 4.13: CFD analysis off the plenum designs.

# Chapter 5

## UC<sup>2</sup>AV Results

### 5.1 UC<sup>2</sup>AV Design

To apply CC on a fixed-wing Class-I UAV, space limitations, weight restrictions and power penalties are important considerations. The ASU is designed to integrate into the fuselage of the UAV, and hence a test platform with sufficient fuselage space is required. Payload capability of the test platform is also an important factor due to the addition of multiple components of the CC system. In addition, the wingspan, wing loading and the chord length are also considered. During the process of selection of a UAV test platform these characteristics are used as comparative parameters between the different platforms.

In comparison to other platforms, the RMRC Anaconda operates at low speeds with high payload capabilities and has a large internal fuselage volume to accommodate the CC system. The UAV is a twin-boom, inverted V-tail configuration; powered by an electric brushless motor driving a pusher type propeller. The aircraft has a maximum payload capability of 1.5 kg and an average cruise speed of 12 m/s at sea level. Selected dimensional parameters of the UAV are presented in Table 5.1. In consideration of all the above parameters, the RMRC Anaconda shown in Figure 5.1 is selected as the CC-test platform.

Table 5.1: Dimensional specifications of the RMRC Anaconda

Fuselage			Wing	
Length	L	800 mm	Mean Chord	238 mm
Max. Internal Height	H	110 mm	Root Chord	280 mm
Max. Internal Width	W	160 mm	Tip Chord	200 mm
			Wing Span	2000 mm



Figure 5.1: The RMRC Anaconda UAV platform.

The RMRC Anaconda platform is modified to accommodate the multiple subsystems to achieve CC on the UAV. Multiple subsystems are integrated aboard the UC<sup>2</sup>AV to achieve CC and to validate the performance of the UAV. The wing on the Anaconda is replaced by a CCW, which follows the airfoil shape of a NACA 0015. The wing is also integrated with Dual Radius Flaps (DRF) investigated by Kanistras et al.[9]. An instrumentation system is added to accurately quantify the performance of the UAV. A CAD model of the UC<sup>2</sup>AV and its multiple sub systems is shown in Figure 5.2.

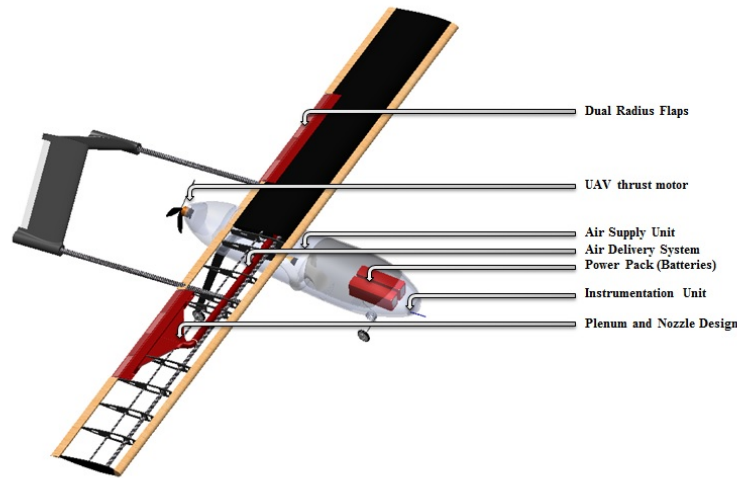


Figure 5.2: The subsystems on-board the UC<sup>2</sup>AV.

### 5.1.1 Circulation Control Wing

A NACA 0015-based CCW is designed by Kanistras et al.[1], consisting of two components: (i) the wing structure; (ii) the pneumatic system inside the wing described in Section [4.4]. The wing structure consist of rods and ribs that are covered by a balsa skin and MonoKote tape. Carbon fiber rods are used to connect and support the ribs along the wingspan. The ribs add strength to the structure and shape the wing section. The skeletal structure of the ribs attached to the skin prevent the structure from buckling or twisting. The ribs also act as mounting points for the control surfaces, flaps and ailerons that are integrated. In addition, the ribs support the plena and pneumatic plumbing located inside the wing. Due to pneumatic piping and plena located inside the wing, the entire wing is assembled as a single unit. The ribs are rapid prototyped out of Acrylonitrile-Butadiene-Styrene (ABS) plastic, two carbon fiber rods and balsa wood the LE and TE are assembled together using CA glue. Figure 5.3 shows the structure of the CCW. Table 5.2 shows the geometric specification of the wing.

Table 5.2: Geometric parameters of the wing[1].

Wing			
Airfoil	NACA0015		
Chord	c	0.24	m
Thickness	t/c	15	%
Camber	m/c	0	%
Angle of Incidence	$\epsilon$	4	$^{\circ}$
Area	S	0.48	m <sup>2</sup>
Wingspan	b	2	m
Half-Span	s	1	m
Aspect Ratio	A	8.33	
Dihedral Angle	$\beta$	0	$^{\circ}$
Sweep Angle	$\Lambda$	0	$^{\circ}$

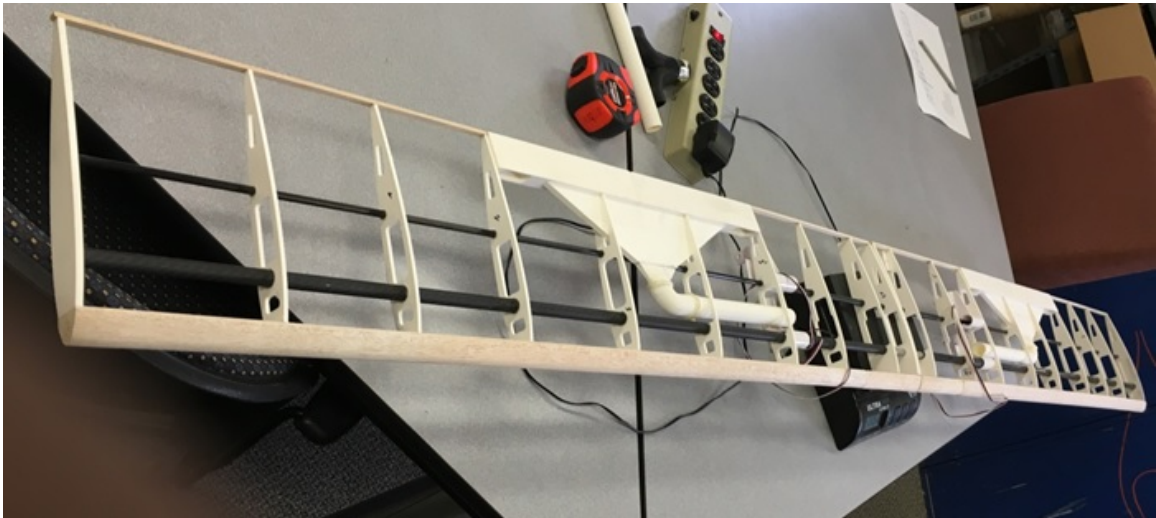


Figure 5.3: The internal structure of the Circulation Control Wing.[1]

### 5.1.2 Flight Controls and Instrumentation

Instrumentation plays an important role in validating the performance of a UAV during flight. However, UAVs often have limited weight and space available, therefore, selection of the right instrumentation is important. The key role of the instrumentation system is to track, characterize and validate the performance of the UAV. A typical flight requires the following data channels: one channel for time stamp (micro-controller); five channels for the pilot's inputs (RC receiver); three channels for pitot sensors (raw data); three channels (Yaw, Pitch, Roll) for inertial Measurement Unit (IMU) orientation; one channel for temperature; one channel for altitude (high range barometric sensor); one channel for low range high accuracy altitude (ultrasonic distance sensor). All data are stored in an on-board SanDisk memory card (32 GB). The data contains a record of the entire flight; however, maneuver markers (set by the pilot with a switch on a spare RC channel) indicate the areas of interest and allow for a quick review of regions of data in the field.

A block diagram of the instrumentation system is shown in Figure 5.4. The measurement of the attitude angles,  $\phi$ ,  $\theta$  and  $\psi$  (roll, pitch and yaw respectively), is performed with a VectorNav VN-100 IMU chip mounted on a development board. This sensor incorporates a 3-axis magnetometer, a 3-axis accelerometer and 3-axis gyroscope with extended Kalman filter. The IMU's outputs include the aircraft attitude expressed as Euler angles or quaternions, linear accelerations, angular rates or magnetic local field. Three pitot probes, each connected to a differential pressure sensor, are located at the front of the fuselage and on either side of the wings to measure true airspeed. To record the altitude and temperature a barometric pressure sensor (Bosch BMP085 transducer mounted on a Sparkfun breakout board) is used. An ultrasonic distance sensor located on the lower front part of the fuselage is used to locate the precise moment that the front wheel becomes airborne. Table 5.3 lists the sensors used on-board the *UC<sup>2</sup>AV* and their specifications.

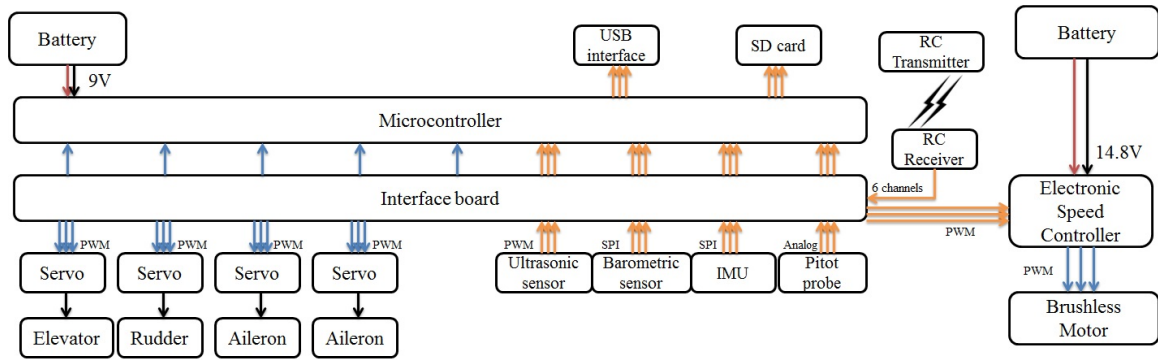


Figure 5.4: Overview of the instrumentation system of the UC<sup>2</sup>AV[1].

Table 5.3: Instrumentation/Sensor Specifications for UC<sup>2</sup>AV[1].

Component	Manufacturer	Part Number	Specifications
Microprocessor	Arduino	Arduino Mega 2560	Microcontroller : Atmega2560 Operating Voltage : 5V Digital I/O Pins : 54 with 15 PWM pins Analog Inputs : 16 Weight : 37 g
RC Transmitter/Receiver	Flysky	FS-i6	Frequency range : 2.405 to 2.475 GHz Number of Channels : 6
Inertial Measurement Unit	Vectornav	VN-100	3-axis accel/gyro/mags. with on-board extended Kalman Filter Gyro range : $\pm 2000$ °/s, linearity <0.1% FS Accelerometer range : $\pm 16$ g, linearity <0.5 % FS Overall weight : 37 g
Pitot Sensors	Freescale Semiconductor	MPXV7002DP	Pressure range : $\pm 2$ kPa Accuracy : 2% FS Sensitivity : 1 V/kPa Response time : 1ms
Barometric Sensor	Bosch Sensortec	BMP085	Pressure range : 30 to 110 kPa RMS noise : 0.1 m Weight : 10 g
Ultrasonic Distance Sensor		HC-SR04	Ultrasonic Frequency : 40 kHz Resolution : 1 cm
Memory Module	Sparkfun OpenLog	Dev-09530	Baud rates : 2400 to 115200

## 5.2 Preflight Tests

Prior to flight tests the CC system is operated by running the ASU and pneumatic system while the UC<sup>2</sup>AV is stationary. The CC system is tested for uniformity to ensure that potential damage within the system does not cause uneven flow across the span. Uniformity plays a crucial role in the the stability around the roll axis of the UAV, this test ensures that the CC system does not introduce undesired instabilities. Also, the momentum coefficient values (based on an average flight velocity of 15 m/s) for different test RPMs are measure and recorded. The pitot used to test the plenum performance in Chapter 4 and speed controller are used to measure and control the CC system performance on-board the UC<sup>2</sup>AV.



Figure 5.5: The UC<sup>2</sup>AV placed on the a stationary mount for platform.

## 5.2.1 Flow Uniformity

CC control is applied to 40% of the span and the plena are located symmetrically on the either side of fuselage at a distance of 250mm to avoid wake effects of the propeller. The flow uniformity across each plenum is evaluated manually. Figure 5.6 presents the performance of each plenum and the deviation of the velocity from the average line (shown in black) at two different (half and full scale RPM). The pitot probe is used to collect 5 points across each plenum designs. The procedure is repeated three times for each RPM, since high flow uniformity and repeatability is essential for the stable operation of the UAV. As seen in the plot, only one point on the left plenum displays a deviation in the jet velocity for both RPM. No significant flow abnormalities in jet velocities are detected.

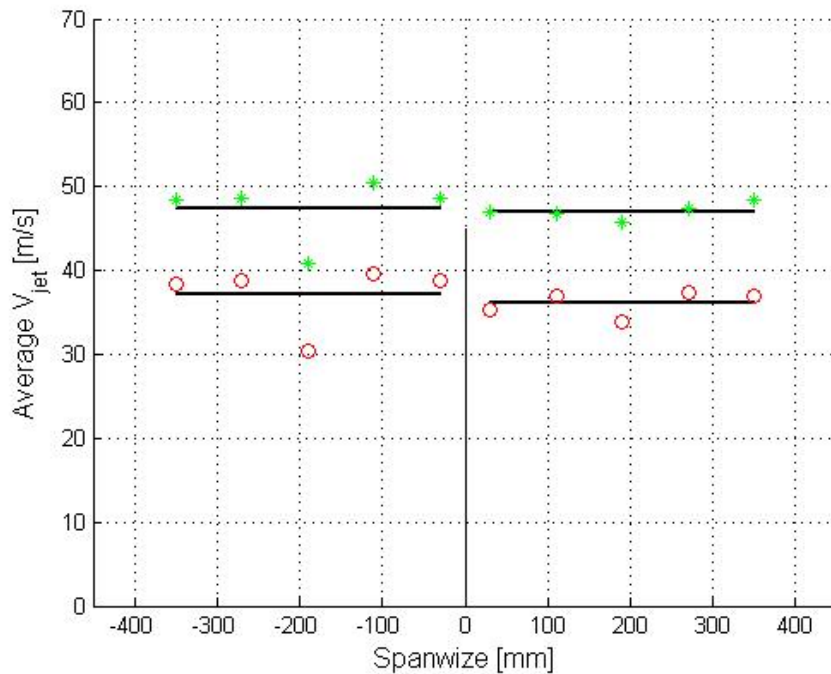


Figure 5.6: Average jet velocity at different points across the span of the UC<sup>2</sup>AV.

### 5.2.2 $C_\mu$ characterization

The momentum coefficient is one of the most significant performance parameters of a CC system and is used to quantify the efficiency of CC. The  $C_\mu$  at the jet is defined as:

$$C_\mu = \frac{Thrust}{q_\infty S} = \frac{\dot{m}_{jet} V_{jet}}{q_\infty S} \quad (5.1)$$

where

$$\dot{m}_{jet} = \rho_{jet} V_{jet} A_{jet} \quad (5.2)$$

The mass flow rate  $\dot{m}_{jet}$  is calculated using Eq. (5.2). The velocity at the jet ( $V_{jet}$ ) is measured as an average jet velocity at the TE of the CCW. The momentum coefficient ( $C_\mu$ ) values are in the range of 0 to 0.045. The  $C_\mu$  vs RPM relation of the UC<sup>2</sup>AV is shown in Figure 5.7. A free stream velocity of 13 m/s is used as an average velocity at take-off.

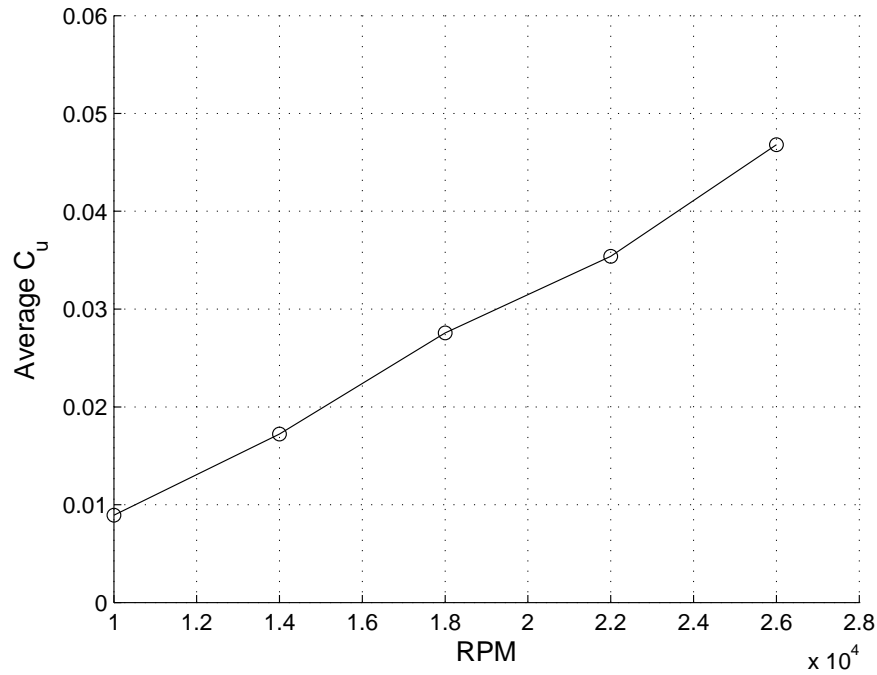


Figure 5.7: The average  $C_\mu$  at different RPM.

## 5.3 UC<sup>2</sup>AV : Flight Results

### 5.3.1 Take-off Characteristics

The take-off performance/characteristics of the aircraft can be estimated within a certain degree of accuracy by analyzing the data as average of multiple runs. With respect to the evaluation of the take-off performance of the UC<sup>2</sup>AV the take-off run of the UAV is divided into two stages: (i) the ground phase; (ii) the air phase. The ground phase of take-off is defined as the time from when the pilot provides thrust input to the UAV, until the plane becomes airborne. The air phase follows the ground phase, and it defined as the portion of flight from the point of take-off until the UAV reaches 50 ft. A graphical representation of the take-off phases is shown in Figure 5.9



Figure 5.8: The UC<sup>2</sup>Av place on the runway prior to take-off..



Figure 5.9: Representation of the ground and air phase of take-off.

To accurately track the take-off distance, three cameras and two observers are positioned at different points along the runway. To ensure that the cameras and observers can accurately capture the take-off point, runway markers are placed every 3 m along the take-off length. On-board the UAV, the ultrasonic sensor measures the exact point of take-off, which helps correlate all the instrumentation data to the exact point of lift-off. A vane anemometer and density/humidity sensor are used to record weather conditions (i.e. runway temperature, humidity, wind condition). Figure 5.10 shows the data that are obtained from the instrumentation during the take-off phase. The first three plots show pitch, roll and the true air speed of the UAV. The pilots inputs are also recorded to ensure unbiased flights; the bottom half of the plots represent this data.

Table 5.4: CC flight test data.

Flight Number	ASU	Dual Radius Flap Deflection (°)	Air Density ( $kg/m^3$ )	Wind Condition	Liftoff Time (s)	Take-off Time (s)	Ground Distance (m)	Air Distance (m)	Take-off Distance (m)	Liftoff Velocity (m/s)	$C_{Lg}$
1	Off	30	0.992	Calm	8.94	13.33	102	78	180	18.2	0.57
2	On	30	1.009	Calm	5.41	12.875	48	115	163	13	1.10
3	On	30	1.016	Calm	6.30	11.67	54	55	109	12.5	1.17
4	Off	30	1.016	Calm	9.8	14.30	117	60	177	-	-
5	On	30	1.002	Calm	-	-	60	-	-	-	-
6	Off	30	1.011	Calm	-	-	93	-	-	-	-
7	On	30	1.011	Calm	-	-	42	-	-	-	-

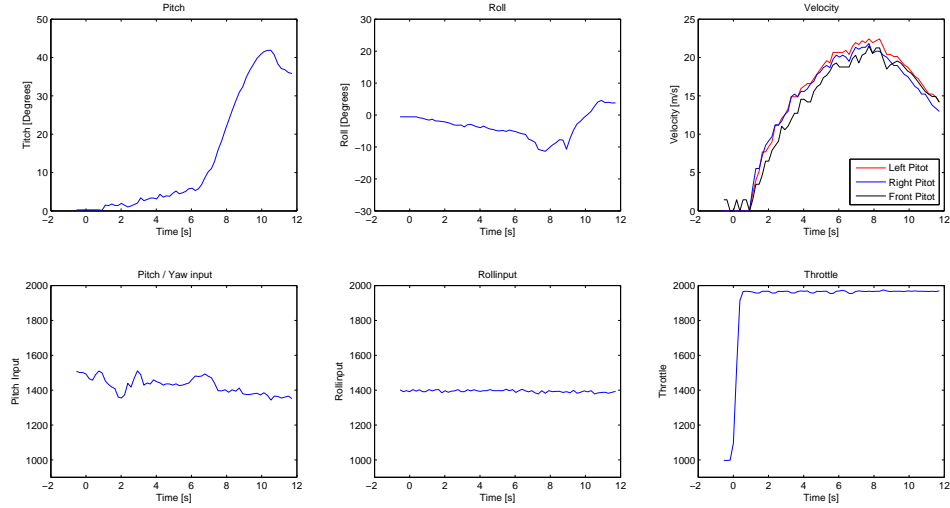


Figure 5.10: Take-off flight data.

A comparative analysis of the flights is conducted to analyze the performance of the CC system on-board the UAV in-terms of the enhancement of performance of the UAV. In all of these flight tests, the ASU is operated at maximum RPM ( $C_{\mu} = 0.165$ ) and is used during the take-off maneuver after which it is turned off. The ASU running at the maximum RPM to achieve the maximum augmented lift to reduce the take-off run. Seven flights are conducted using the UC<sup>2</sup>AV, all flights are from the same day under similar weather conditions. As a malfunction in the instrumentation system occurred after the third flight, the data collected from that point on are analyzed using videos and observers during the ground phase. The take-off weight of the UC<sup>2</sup>AV is 4.7 kg (10.36 lbs). The data presented in Table 5.4 indicate that CC is effective and can reduce the ground distance up to 53 %. A comparison between the first and second flight shows that the lift coefficient on the ground, using the CC system the lift co-efficient can be enhanced by 93%. Further details of the flights and analysis of the results are described in [1].

The importance of these results is best evaluated in comparison with previous work in the field detailed in literature review. Published flight data that confirms CC being applied

on an unmanned fixed wing aircraft to achieve short take-off envelopes (reduced ground distance) do not exist. While additional tests must be carried out to check for repeatability of the system performance at different condition, the collected data is sufficient to confirm that CC system can successfully meet the pneumatic needs of the UC<sup>2</sup>AV. Significant runway reduction is achieved with low power penalties and low blowing rates using the CC system developed during the course of this thesis.

# Chapter 6

## Conclusions and Future Work

### 6.1 Conclusions

In this research, a novel CC system for a Class-I UAV is designed and evaluated. The primary function of the CC system is to achieve a high velocity jet at the trailing edge of a Circulation Control Wing, thus enabling improved performance. The presented thesis establishes the foundations and technical details of design, development and computational/experimental testing of the CC system.

A detailed design and aerodynamic study is conducted on a light weight air supply unit, capable of supplying the required mass flow for CC applications. Rapid prototyping is used to manufacture a light weight compressor weighing 95 grams, which is capable of providing a Flow Rate ( $Q$ ) of  $0.037 \text{ m}^3/\text{s}$  at a maximum tested RPM of 26000. Detailed experimental/computational testing of the flow rates, power consumption and pressure ratio are characterized. A computational analysis is conducted to validate the experimental results and study the internal flow field. A CC system is consisting of a plenum for flow distribution along the wing span, pneumatic tubing and an inlet junction integrable with the ASU and the UC<sup>2</sup>AV are designed and tested. The complete CC system weighing 650 g

(1.433 lbs) is capable of providing the mass flow to the CCW. The CC system is integrated on the UC<sup>2</sup>AV along with Dual Radius Flaps and instrumentation system. The flight testing of the UC<sup>2</sup>AV demonstrates that the use of Circulation Control can successfully be applied to Class-I UAVs, despite the space and power constraints. In conclusion, the CC system developed and integrated on-board the UC<sup>2</sup>AV successfully enhances the aerodynamic performance of the airplane while reducing take-off distances.

## 6.2 Future Work

The research carried out in this dissertation can be advanced in three directions: change of manufacturing methods and materials, application of the CC system for a multiple plenum based wing to provide the benefits of CC over the entire wing and test for scalability of the system for its applications towards manned aircraft. Through the entire research the manufacturing was restricted by the weight restrictions on-board the UAV and the ASU and pneumatic system were manufactured through rapid prototyping using ABS plastic. However, future developments to this work may use high precision tooling methods (CNC milling) and the use of light weight metal alloys to achieve better tolerances can be investigated. CC on-board the UC<sup>2</sup>AV was only applied to 40% of the wingspan. Future work can include modification of the pneumatic system to achieve CC on the entire span of the wing to further improve the performance of the plane. Since centrifugal compressors are scalable within the same range of Reynolds numbers, the ASU can be scaled-up to meet the additional flow rate requirement of such a system and for applications on personal air vehicles and larger UAVs.

# Bibliography

- [1] K. Kanistras, S. P. Chander, K. P. Valavanis, and M. J. Rutherford, *UC2AV Unmanned Circulation Control Aerial Vehicle for Short Takeoff and Enhanced Payload*. 34th Applied Aerodynamics Conference, AIAA Aviation, Washinton DC, 2016.
- [2] R. Sparks, S. Michie, and K. Gill, *Development of an Integrated Circulation Control Fluidic Thrust Vectoring Flight Test Demonstrator*. 1st International Conference on Innovation and Integration in Aerospace Sciences, Queen's University Belfast, Northern Ireland, UK, 2005.
- [3] G. A. I. Monterzino and C. P. Lawson, *Development of a Pneumatic System to Enable Flight without Conventional Control Surfaces*. 27th International Congress of the Aeronautical Sciences, Nice France, 2010.
- [4] N. R. Alley, J. Steele, J. C. Neidhoefer, R. J. Englar, and G. Blaylock, *Development of a Cruise-Efficient Extreme-STOL-Capable Demonstrator UAV*. AIAA Infotech@Aerospace 2010 20 - 22 April 2010, Atlanta, Georgia, 2010.
- [5] W. C. Horne and N. J. Burnside, *AMELIA CESTOL Test: Acoustic Characteristics of Circulation Control Wing and Leading- and Trailing-Edge Slot Blowing*. 51st AIAA Aerospace Science Meeting including the New Horizons Forum and Aerospace Exposition, Dallas, Texas, 2013.
- [6] W. E. Milholen, G. S. Jones, D. T. Chan, S. L. Goodliff, S. G. Anders, L. P. Melton, M. B. Carter, B. G. Allan, and F. J. Capone, *Enhancements to the FAST-MAC Circulation Control Model and Recent High-Reynolds Number Testing in the National Transonic Facility*. 31st AIAA Applied Aerodynamics Conference San Diego CA, 2013.

- [7] M. P. Boyce, *Principles of Operation and Performance Estimation Of Centrifugal Compressors*. Twenty Second Turbo Machinery Symposium, Houston, Texas, 1993.
- [8] P. C. Saka, K. Kanistras, M. J. Rutherford, and K. P. Valavanis, *Development of a Framework for a Circulation Control-Based Unmanned Aerial Vehicle*. IEEE Aerospace Conference, Montana, 2016.
- [9] K. Kanistras, P. C. Saka, K. P. Valavanis, N. Vitzilaios, and M. J. Rutherford, *Experimental Study of Circulation Control Wings at Low Reynolds Numbers*. 33rd Applied Aerodynamics AIAA Aviation Conference, Dallas, 2015.
- [10] A. Buonanno and M. V. Cook, *Flight Dynamic Simulation of a Flapless Flight Control UAV*. 25th International Congress of the Aeronautical Sciences, Hamburg, Germany, 2006.
- [11] K. K. Jameson, D. D. Marshall, R. Ehrmann, E. Paciano, R. Golden, and D. Mason, *Design and Wind Tunnel Testing of CAL POLY's AMELIA 10 Foot Span Hybrid Wing-Body Low Noise CESTOL Aircraft*. 27th International Congress of the Aeronautical Sciences, Nice France, 2010.
- [12] R. J. Englar, *Development of the A-6/Circulation Control Wing Flight Demonstrator Configuration*. David W. Taylor Naval Ship Research and Development Center, Bethesda, MD, 1979.
- [13] R. J. Englar, *Circulation Control Pneumatic Aerodynamics: Blown Force and Moment Augmentation and Modification; Past, Present and Future*. AIAA Paper, 2000-2541, presented at AIAA Fluids 2000 Meeting, Denver, CO, 2000.
- [14] R. J. Englar and R. M. Williams, *Design of Circulation Controlled Stern Plane for Submarine Applications*. David Taylor Naval Ship R&D Center Report NSRDC/AL-200 (AD901-198), 1971.
- [15] K. Kanistras, M. J. Rutherford, and K. P. Valavanis, *Development of a Circulation Control Wing for UAVs*. IEEE Aerospace Conference, Montana, 2014.
- [16] G. S. Jones and R. J. Englar, *Advances In Pneumatic-Controlled High-Lift Systems Through Pulsed Blowing*. AIAA Paper 2003-3639 NASA techdocs, 2003.

- [17] K. C. Pfingsten and R. Radespiel, *Experimental and numerical investigation of a circulation control airfoil*. 47th AIAA Aerospace Sciences Meeting Including The New Horizons Forum and Aerospace Exposition, Orlando, Florida, 2009.
- [18] J. B. Montanya and D. D. Marshall, *Circulation Control and its Application to Extreme Short Take-Off and Landing Vehicles*. 45th AIAA Aerospace Sciences Meeting and Exhibit, Reno, NV, 2007.
- [19] E. N. Paciano, J. A. Lichtwardt, D. D. Marshall, K. K. Jameson, and R. K. Fong, *Flow Uniformity Calibration of AMELIA's Circulation Control Wings*. 51st AIAA Aerospace Science Meeting including the New Horizons Forum and Aerospace Exposition, Dallas, Texas, 2013.
- [20] G. S. Jones, W. E. Milholen, D. T. Chan, B. G. Allan, S. L. Goodliff, L. P. Melton, S. G. Anders, M. B. Carter, and F. J. Capone, *Development of the Circulation Control Flow Scheme used in the NYF Semi-Span FAST-MAC Model*. 31st AIAA Applied Aerodynamics Conference San Diego CA, 2013.
- [21] T. Hideaki, U. Masaru, K. Tomoki, and H. Yutaka, *Aerodynamic Design of Centrifugal Compressor for AT14 Turbocharger*. —H— Engineering review Vol . 43 No. 2 2010, 2010.
- [22] S. Ibaraki, I. Tomita, M. Ebisu, and T. Shiraishi, *Development of a Wide-Range Centrifugal Compressor for Automotive Turbochargers*. Mitsubishi Heavy Industries Technical Review Vol. 49 No. 1, 2012.
- [23] K. Kanistras, M. J. Rutherford, N. Vitzilaios, and K. P. Valavanis, *Experimental Study of Circulation Control Wings at Low Reynolds Numbers*. 32nd Applied Aerodynamics Conference, AIAA Aviation, Atlanta, 2014.
- [24] D. L. Palmer and W. F. Waterman, *Design and Development of an Advanced two-stage Centrifugal Compressor*. ASME 94-GT-202, 1994.
- [25] M. M. Rahman and R. P. Scaringe, *Performance Evaluation of Small Centrifugal Compressors for Application in Air-Cycle Power and Refrigeration System*. International Compressor Engineering Conference, Purdue University Purdue e-Pubs, Paper 819, 1992.

- [26] Al-Zibaidy, A *Proposed Design Package for Centrifugal Impellers*. Computers and Structures, Elsevier Vol. 55. No. 2, pp. 347-356, 1995.
- [27] D. P. S. Abam and E. G. Saturday, *Optimization of Centrifugal Compressors : A Case Study*. Journal of Emerging Trends in Engineering and Applied Sciences (JETEAS) 3(4) 688-694 (ISSN: 2141-7016), 2012.
- [28] A.-S. A. Fahd and A.-Q. M. Amro, *Design of Small Centrifugal Compressors Performance Test Facility*. ASME Turbo Expo, Vienna, Austria, 2004.
- [29] V. V. Prasad, M. L. Kumar, and B. Reddy, *Centrifugal Compressor Fluid Flow Analysis using CFD, Vol 1, No. 1, pp:6-10*. Science Insight: An international Journal, 2011.
- [30] A. Oyelami, S.B.Adejuyigbe, M. Waheed, A. Ogunkoya, and D. Illaya, *Analysis of Radial-Flow Impellers of Different Configurations*. The Pacific Journal of Science and Technology, Vol 13, No. 1, pp. 24-33, 2012.
- [31] R. N. Brown and R. A. Lewis, *Centrifugal Compressor Application Sizing, Selection and Modelling*. Twentieth Turbomachinery Symposium, Texas, USA, 1991.
- [32] N. Madhwesh, K. V. Karanth, and N. Y. Sharma, *Impeller Treatment for a Centrifugal Fan Using Splitter Vanes - A CFD approach*. World congress on engineering, 2011.
- [33] M. Zangeneh, B. Nikpour, and H. Watanbe, *Development of a high performance centrifugal compressor using 3D inverse design technique*. 9th International Conference on Turbochargers and Turbocharging, May 19-20, London, Uk, 2010.
- [34] K. Kanistras, S. P. Chander, K. P. Valavanis, and M. J. Rutherford, *Low Speed Wing Tunnel Investigation of a Circulation Control Wing for Enhanced Lift*. 33rd Applied Aerodynamics Conference, AIAA Aviation, Dallas, 2015.
- [35] S. K. Kurauchi and J. R. Barbosa, *Design of a Centrifugal Compressor for Natural Gas*. The 14th Brazilian Congress of Thermal Sciences and Engineering, Rio de Janeiro,RJ,Brazil, 2012.
- [36] J. H. Perry and C. H. Chilton, *Chemical Engineers' Handbook*. McGraw-Hill book Comp., 1963.

- [37] R. D. Blevins, *Applied Fluid Dynamics Handbook*. Krieger Pub., 2003.
- [38] I. E. Idel'chik, *Design of Fluid Thermal Systems*. U.S. Department of Commerce Clearinghouse for Federal Scientific and Technical Information Springfield, Va. 22151, 1986.
- [39] W. S. Janna, *Handbook of Hydraulic Resistance*. CL Engineering, 2nd edition, 1998.
- [40] E.N.Paciano, J.A.Lichtwardt, D.D.Marshall, K.K.Jameson, and R.K.Fong, *Flow Uniformity Calibration of AMELIAs Circulation Control Wings*. 51st AIAA Aerospace Sciences Meeting including the New Horizons Forum and Aerospace Exposition, Dallas, Texas, 2013.
- [41] G.S.Jones, W.E.Milholen, D.T.Chan, B.Allan, S.L.Goodliff, L.Melton, S.G.Anders, M.Carter, and F.Capone, *Development of the Circulation Control Flow Scheme used in the NTF Semi-Span FAST-MAC Model*. 31st AIAA Applied Aerodynamics Conference, San Diego, CA, 2014.